MIT Open Access Articles

Hydrogel-based biocontainment of bacteria for continuous sensing and computation

Check for updates

Hydrogel-based biocontainment of bacteria for continuous sensing and computation

Tzu-Chieh Tang [1,2,3,17] ✉, Eléonore Tham[1,4,17], Xinyue Liu[5,17], Kevin Yehl[1,2,13], Alexis J. Rovner[6,7], Hyunwoo Yuk [5], Cesar de la Fuente-Nunez[14,15,16], Farren J. Isaacs[8,9,10], Xuanhe Zhao[5,11] ✉ and Timothy K. Lu [1,2,12] ✉

Genetically modified microorganisms (GMMs) can enable a wide range of important applications including environmental sensing and responsive engineered living materials. However, containment of GMMs to prevent environmental escape and satisfy regulatory requirements is a bottleneck for real-world use. While current biochemical strategies restrict unwanted growth of GMMs in the environment, there is a need for deployable physical containment technologies to achieve redundant, multi-layered and robust containment. We developed a hydrogel-based encapsulation system that incorporates a biocompatible multilayer tough shell and an alginate-based core. This deployable physical containment strategy (DEPCOS) allows no detectable GMM escape, bacteria to be protected against environmental insults including antibiotics and low pH, controllable lifespan and easy retrieval of genomically recoded bacteria. To highlight the versatility of DEPCOS, we demonstrated that robustly encapsulated cells can execute useful functions, including performing cell–cell communication with other encapsulated bacteria and sensing heavy metals in water samples from the Charles River.

Genetically modified microorganisms (GMMs) are being developed and used for bioremediation[1], agriculture[2] and the production of engineered living materials and devices[3]. However, the potential for GMMs to escape into the environment has created a need for strategies to contain these organisms and prevent their uncontrolled release[4,5].

Chemical biocontainment uses chemical barriers to impede the escape and survival of microorganisms in the environment[4,6]. Several strategies have been developed for chemical containment of GMMs[7,8]. For example, GMMs can carry genetic circuits that require specific chemical combinations to prevent cell death by inhibiting toxin production[9], rescue cells from being killed by a constitutively expressed toxin by producing the corresponding antitoxin[10] or multi-layered safeguards that modulate the expression of essential genes and toxins[11]. In addition, microbes can be engineered with auxotrophies so that they require synthetic amino acids for survival[12]. However, chemical strategies alone are imperfect for containment because mutation rates of GMMs, while low, are never zero, thus resulting in escape mutants. This indicates that the number of chemically contained GMMs that can be deployed is intrinsically limited by their mutation rate[12]. Thus, it would be beneficial to combine biological containment strategies and physical encapsulation such that functional redundancy further reduces any chance of inadvertent escape.

To address this challenge, we created a deployable physical containment strategy (DEPCOS), which prevents GMM escape while providing a tunable protective environment in which GMMs can execute engineered functions. DEPCOS erects a physical barrier to prevent GMMs from escaping into their surroundings, limit HGT between GMMs and natural species in the environment, and allow for easy retrieval of bacterial communities.

Hydrogels are desirable materials for encapsulating living cells as they provide an aqueous environment that can be infused with nutrients, allowing for cell growth[13] and sensing[14], while also protecting against environmental hazards[15]. Alginate forms hydrogels in the presence of di-cationic solutions (for example, Ca^{2+}, Ba^{2+}) and has been used in various biomedical applications[16,17] because of its low cost, negligible cytotoxicity and mild gelation conditions. However, weak mechanical properties and susceptibility to multiple chemical conditions (such as low pH, citrate and phosphate) make alginate, as well as other traditional hydrogels, poor solutions for robust physical containment when used on their own[18–20].

Core-shell designs that include an alginate core and a polymer-based protective shell have emerged as potential design

[1]Synthetic Biology Group, Research Laboratory of Electronics, Massachusetts Institute of Technology, Cambridge, MA, USA. [2]Department of Biological Engineering, Massachusetts Institute of Technology, Cambridge, MA, USA. [3]The Mediated Matter Group, Media Laboratory, Massachusetts Institute of Technology, Cambridge, MA, USA. [4]Department of Materials Science and Engineering, Massachusetts Institute of Technology, Cambridge, MA, USA. [5]Department of Mechanical Engineering, Massachusetts Institute of Technology, Cambridge, MA, USA. [6]Wyss Institute for Biologically Inspired Engineering, Boston, MA, USA. [7]Department of Genetics, Harvard Medical School, Harvard University, Boston, MA, USA. [8]Department of Molecular, Cellular and Developmental Biology, Yale University, New Haven, CT, USA. [9]Systems Biology Institute, Yale University, West Haven, CT, USA. [10]Department of Biomedical Engineering, Yale University, New Haven, CT, USA. [11]Department of Civil and Environmental Engineering, Massachusetts Institute of Technology, Cambridge, MA, USA. [12]Department of Electrical Engineering and Computer Science, Massachusetts Institute of Technology, Cambridge, MA, USA. [13]Present address: Department of Chemistry and Biochemistry, Miami University, Oxford, OH, USA. [14]Present address: Machine Biology Group, Departments of Psychiatry and Microbiology, Institute for Biomedical Informatics, Institute for Translational Medicine and Therapeutics, Perelman School of Medicine, University of Pennsylvania, Philadelphia, PA, USA. [15]Present address: Departments of Bioengineering and Chemical and Biomolecular Engineering, School of Engineering and Applied Science, University of Pennsylvania, Philadelphia, PA, USA. [16]Present address: Penn Institute for Computational Science, University of Pennsylvania, Philadelphia, PA, USA. [17]These authors contributed equally: Tzu-Chieh Tang, Eléonore Tham, Xinyue Liu. ✉e-mail: zijaytang@gmail.com; zhaox@mit.edu; timlu@mit.edu
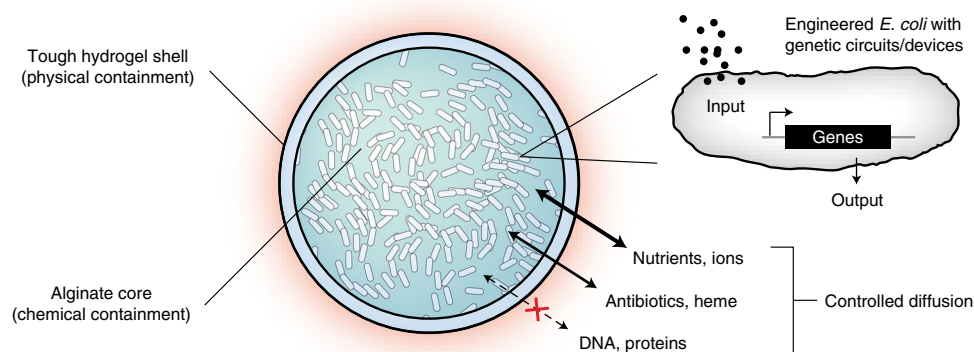
Fig. 1 | Schematic of the DEPCOS platform. The DEPCOS platform provides secure biocontainment by using a core-shell hydrogel design. The tough and semipermeable hydrogel shell provides a confining barrier for physical containment and protection against insults. The alginate-based hydrogel core contains nutrients for microbial growth and survival, enabling chemical containment. Engineered cells equipped with genetic circuits receive environmental inputs and generate desirable outputs. Nutrients, biomolecules and other analytes selectively diffuse into and out of the bead depending on molecular weight and charge.

for alginate-based microbial biosensors[19,21]. Nonetheless, there is a major need for a mechanically tough shell that is also highly permeable to analytes for sensing. Our DEPCOS design for bacterial encapsulation consists of two parts: (1) an alginate-based hydrogel core and (2) a tough hydrogel shell (Fig. 1) that combines both a stretchy polymer network (polyacrylamide) and an energy dissipation network (alginate, through the unzipping of ionic crosslinking between polymer chains)[22]. This shell material is extremely tough and resistant to fracture, yet retains permeability to small molecules[23]. Herein, we test the biocompatibility of this hydrogel and further expand on its physical characterization for core-shell particle form factors. By combining physical and chemical containment strategies, the DEPCOS platform enables near-perfect biocontainment and protects the encapsulated cells from environmental insults. Various engineered bacterial strains hosting genetic circuits for sensing, recording and communication operate robustly in a plug-and-play fashion with DEPCOS. This study demonstrates the potential of using dual-mode biocontainment for the real-world deployment of GMMs powered by synthetic biology.

Results

Manufacturing the DEPCOS hydrogel beads. To incorporate living cells into the particle core, liquid cultures of *Escherichia coli* were mixed with alginate in 50- or 100-μl droplets that were crosslinked with calcium ions to form spheres. The cell-containing alginate hydrogel was easily shaped by a mold or cut into different geometries (Supplementary Fig. 1). Cores were then coated with the tough polyacrylamide-alginate hydrogel layer[22] (Fig. 2). In our core-shell system, the alginate core is preloaded with nutrients to support growth while the hydrogel shell provides mechanical protection for the entire bead. For downstream analyses after deployment, cells can easily be retrieved from the beads by removing the shell with a razor blade and homogenizing the core (Supplementary Fig. 2). Due to the observed toxicity of the chemical crosslinkers (Supplementary Fig. 3), a 12-hour outgrowth step was performed to replenish the colony forming units (CFU) count before the following experiments (Supplementary Fig. 4).

Tough hydrogel shell enables robust physical containment. We hypothesized that the tough hydrogel layer would serve as a containment mechanism because its pore size (5–50 nm) is too small for *E. coli* to penetrate[24]. To test this hypothesis, we measured the containment efficiency of hydrogel beads by incubating *E. coli*-encapsulated

beads at the optimal temperature for bacterial growth (37 °C) with shaking. Specifically, we encapsulated a concentration of roughly 10^9 bacteria per ml in each bead. Beads lacking a tough shell allowed bacteria to escape into the surrounding media and to grow to high densities after overnight incubation, whereas there was no physical escape of bacteria from coated beads even after 72 h of incubation (Fig. 3a and Supplementary Fig. 5). In this assay, we plated all of the media (5 ml) surrounding the beads, with a lower limit of detection (LLOD) of 1 CFU in 5 ml. Furthermore, the tough hydrogel shell maintained zero escape under physical insult such as prolonged shaking at 200 r.p.m., outperforming alginate and agarose, two common coating materials for core-shell cell encapsulation (Supplementary Fig. 6).

Next, we used compression testing to characterize the mechanical robustness of the hydrogel-bacteria beads (radius of 3–4 mm) with varying shell layers. We found that beads with a single-layer shell coating (Supplementary Fig. 7) could sustain 25% compressive strains and forces up to roughly 0.1 N before fracture occurred (Fig. 3b and Supplementary Fig. 8a). We further improved the mechanical properties of the beads by creating multilayer shells via repetitive coating. With beads that were coated with three layers of tough polyacrylamide-alginate hydrogel, we did not observe any fracture when the beads were subjected to up to 85% compressive strains and forces up to roughly 3.3 N (Fig. 3b and Supplementary Fig. 8a). The bead capsules were also subjected to cyclic compression at 70% strain, revealing a pronounced hysteresis due to plastic deformation and energy dissipation (Fig. 3c and Supplementary Fig. 8b). Based on the dimensions of the beads, the cyclic effective compressive stress was calculated as roughly 70 kPa (Supplementary Fig. 8b), which is equivalent to pressure at roughly 7 m deep under water and roughly 4 m deep under dry soil[25], and is comparable to that of our previously published ingestible hydrogel device[26]. This result indicates that these beads could sustain stresses much stronger than the maximum gastric pressure (roughly 10 kPa)[27], highlighting their potential for in vivo biosensing. Thus, multilayer coating with elastic tough hydrogel around an alginate core provides mechanical robustness to the entire capsule, a phenomenon that is observed with other stiff polymer coatings[28]. No CFU counts were detected when plating the surrounding media that was incubated with compressed single- and triple-coated beads, suggesting that the capsules withstood successive compressions without fracturing and maintained the level of containment needed for safe environmental deployment
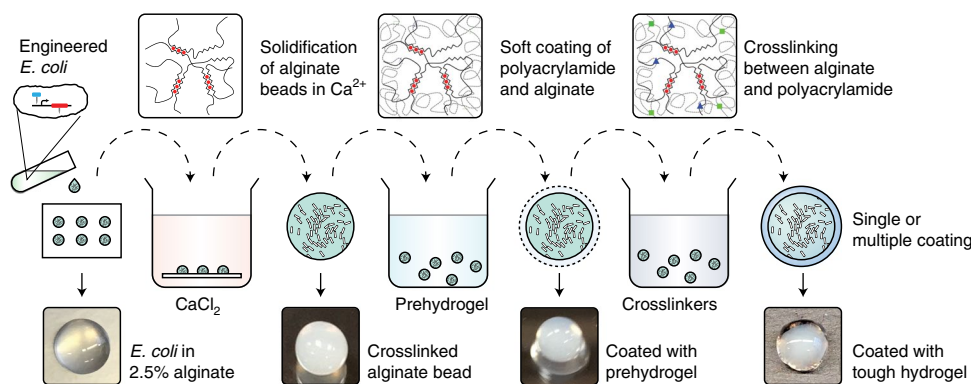
Fig. 2 | Cell encapsulation in tough hydrogel capsules. The process of core-shell encapsulation of cells. Droplets of 2.5% alginate with engineered *E. coli* were crosslinked in a calcium solution to form the soft core of the beads, which were then coated with a layer of alginate/polyacrylamide to form a tough hydrogel shell. The process can be repeated to achieve multiple coatings.

(Fig. 3c, inset). In the liquid environment, the beads showed roughly 25% swelling after day 1 and remained stable over the course of 14 days (Supplementary Fig. 9a). This swelling has a limited impact on the beads' mechanical properties measured by compression (Supplementary Fig. 9b). However, swelling might be a potential challenge for long-term deployment in a low-salt environment and could be minimized by replacing the salt-sensitive alginate with swelling-resistant PEG-containing hydrogels[29].

Synergistic dual-mode containment ensures zero escape. Since extreme forces could potentially compromise our hydrogels and permit bacterial escape, we hypothesized that chemical containment could be used to enforce an additional layer of control over encapsulated cells. Genomically recoded organisms (GROs, microbes with synthetic auxotrophies)[12] can be contained because the growth of these microbes is dependent on the supply of synthetic amino acids (enabling a permissive environment). Here, we sought to combine physical and chemical strategies for biocontainment by encapsulating two GROs auxotrophic for the synthetic amino acid p-iodo-L-phenylalanine (pIF, β) in tough hydrogel beads. The *E. coli* strains rEc.β.dC.12'.ΔtY (mutation rate $<4.9 \times 10^{-12}$) and LspA.Y54β (mutation rate 1.86×10^{-5}) have amber codons inserted in three (*lspA*, *dnaX*, *secY*) and in one (*lspA*) essential genes[12], respectively, to restrict growth to permissive media (containing pIF). We showed that: (1) chemical containment in the beads enables programmable loss of cellular viability after 48 h, which prevents undesirable growth once a given time frame has expired and (2) physical containment adds another layer of protection over chemically contained microbes, which is necessary for applications that require extremely high standards of biocontainment.

First, beads encapsulating the pIF-auxotroph GROs, rEc.β.dC.12'.ΔtY and LspA.Y54β were presoaked in LB in the absence (nonpermissive media) or presence (permissive media) of 1 mM pIF and 0.2% L-arabinose (L-ara), which is required for the expression of aminoacyl-transfer RNA synthetases in these strains[12]. We hypothesized that in nonpermissive media, the GROs would be unable to synthesize functional essential proteins and thus lose viability. Indeed, beads presoaked in nonpermissive media failed to sustain cell growth and showed less than 10% survival after 12 h in LB only (Fig. 4a, cells were plated on permissive solid media), with no survival detected at 24 h. On the other hand, presoaking encapsulated beads in permissive media greatly prolonged cell survival. Greater than 50% of the rEc.β.dC.12'.ΔtY population and >25% of the LspA.Y54β population remained viable after 24 h of incubation. Nearly all cells (>99%) lost viability after 2 d of incubation, which we believe is due to pIF and L-ara depletion by cells, as well as passive diffusion

of these molecules out of the encapsulated hydrogel. Because many chemical induction and sensing responses in *E. coli* require less than 24 h to complete, this defined survival window could be used to prevent the undesirable growth of cells on completion of tasks.

We demonstrated the benefit of combining physical and chemical containment by placing beads in nonpermissive liquid media and then plating samples from the liquid media on nonpermissive solid media. This experiment allowed us to screen for escape mutants. For beads with tough hydrogel coating encapsulating either GRO strain (1.2×10^7 cells), no viable cells were observed in the surrounding nonpermissive media at the end of a 3-day shaking incubation period, indicating complete containment (Fig. 4b). When rEc.β.dC.12'.ΔtY cells (low mutational escape rate, $<4.9 \times 10^{-12}$)[12] were encapsulated in beads without the tough hydrogel coating, no viable cells were observed in the nonpermissive media. On the other hand, when LspA.Y54β cells (higher mutational escape rate, roughly 1.86×10^{-5})[12] were encapsulated in beads without the tough hydrogel coating, mutational escape was observed and cells grew in the nonpermissive media. These results demonstrate that physical containment can complement chemical containment strategies to achieve near-zero escape rates (chemical plus physical). These results suggested that we may be able to program a 'biological timer' system that ceases to grow in the absence of artificial chemicals and eliminates potential bacterial growth outside the bead even when the hydrogel shell is compromised.

DEPCOS prevents DNA transfer and protects GMMs. Horizontal gene transfer (HGT) of engineered genes into the environment and disruption of native ecosystems area major regulatory concerns regarding the deployment of GMMs. Since DNA is much smaller than bacteria, we sought to explore whether DEPCOS could prevent HGT. We used a bacterial conjugation assay (Fig. 4c) where the conjugation efficiency of an F-plasmid carrying a chloramphenicol (Cm) resistance from an F+ donor strain was measured for transfer into a recipient bacteria strain (F−) that lacks Cm resistance. In liquid media, we measured conjugation efficiency to be roughly 1%. When the F+ donor strain was encapsulated within tough hydrogel beads and incubated with recipient bacteria in the surrounding media (2 ml), no transconjugants were detected after 24 h of coincubation (LLOD 1 CFU per 2 ml). In additional to conjugation, GMM-derived DNA might reach the environment through diffusion from decayed GMMs after cell death. We encapsulated DNA molecules at high concentration (3×10^9 copy μl^{-1}) in the beads and measured DNA copy number in the surrounding media using quantitative PCR (qPCR). There was no leakage of DNA molecules as they were perfectly contained (Supplementary Fig. 10) by the
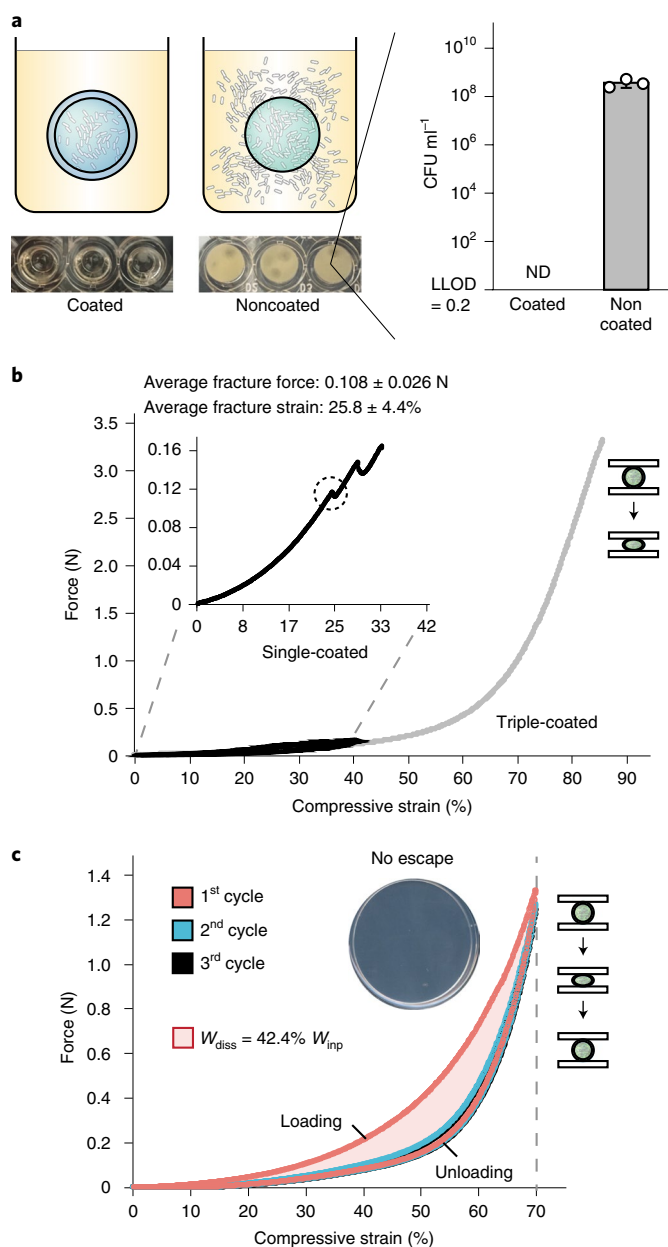
Fig. 3 | Tough hydrogel shell provides robust biocontainment.
a, Encapsulated bacteria escaped from noncoated beads at high rates but did not escape from tough hydrogel-coated beads at detectable levels after 72 h. Inset shows media in which noncoated and coated beads were grown for 24 h (LLOD = 1 CFU per 5 ml). ND, not detectable. Samples prepared in triplicate, data represent the mean ± 1 s.d. **b**, Typical force–displacement curves of single-layer tough hydrogel-coated beads subjected to 40% (black) compressive strain and triple-coated beads subjected to compression up to 85% (gray) compression. Inset zooms in on the single-coated bead stress–strain curve. The average maximum strain and force before fracture for the single-layer coating were 25.8% and 0.108 N, respectively. Triple-coated beads showed no fracture under compression. Samples prepared and measured independently from $n = 14$ beads. **c**, Cyclic compression of triple-layer coated beads showed hysteresis in the stress–strain curve between the first and second cycles due to plastic deformation. Work dissipated W_{diss} in the first cycle was calculated as 42.4% of the total work W_{inp}. Stress–strain curves are representative of at least six independent experiments. Inset shows there was no escape: plating the surrounding media of a bead after cyclic compression yielded no colonies. Samples prepared in triplicate.

alginate-containing DEPCOS, which effectively blocked the diffusion of large biomacromolecules such as DNA[30].

We then investigated the protective effects of the beads on bacterial cells by comparing the resistance of encapsulated cells versus planktonic cells (without bead encapsulation) to a series of chemical and biological stresses (Fig. 4d). Encapsulated bacteria survived to a much greater extent than planktonic cells in the presence of the aminoglycoside antibiotic kanamycin. Encapsulation also helped cells survive acidic environments (pH 4). Such protection became more prominent as the size of the alginate core increased, because the killing was localized near the surface of the alginate core (Supplementary Fig. 11). Thus, our robust hydrogels can prevent bacterial conjugation-based HGT and enhance GMM survival in certain stressful conditions.

Sensing, recording and communication by genetic devices. During the outgrowth step (Supplementary Fig. 4), the number of cells in the beads increased by roughly 10^5-fold (roughly 16–17 doublings) and reached stationary phase after 12 h of incubation, corresponding to a doubling time of roughly 40 min. These data indicate that bacterial cells within the beads are metabolically active and able to divide in the alginate core, which is important for GMMs that must carry out active biological functions[31].

The nanoporous structures of the hydrogel shell and alginate core should allow rapid diffusion of small molecules and ions[16,32] while blocking the passage of large biopolymers such as DNA (Supplementary Fig. 10) and proteins[16]. The anionic nature of alginate in both components further restrict the diffusion of highly charged molecules such as tobramycin[33] and kanamycin (Fig. 4d). Combining the tough hydrogel shell and the alginate core as a whole system, we observed that mildly charged small molecules quickly diffused into the beads (Supplementary Fig. 12), which also suggests that the H^+ ions could diffuse at an even faster rate. To determine whether encapsulated bacteria can respond to these stimuli, we encapsulated bacteria containing a genetic construct that expresses green fluorescence protein (GFP) in response to anhydrotetracycline (aTc) induction. We then incubated the beads at 37 °C in the absence of aTc or in the presence of 200 ng ml^{-1} aTc. We found that encapsulated cells exposed to aTc exhibited a 35-fold increase in green fluorescence compared with encapsulated cells not exposed to aTc, which was lower than the fold induction seen in liquid cultures (Extended Data Fig. 1a), potentially due to limited diffusion within the core. Thus, gene expression in cells encapsulated in tough hydrogels can be exogenously controlled by chemical inducers. In addition, activation of gene expression could still be observed in ready-to-use beads stored at 4 °C for 14 d (Supplementary Fig. 13), which is comparable to current state-of-the-art whole-cell biosensors for field applications[34,35], such as hydrogel-based[20,36] and liquid-in-a-cartridge devices[37]. Additionally, to demonstrate the sensing versatility of our system, we showed that a larger and more charged molecule (heme, physiological charge 3$^+$) with physiological importance could be easily detected using an engineered probiotic *E. coli*[38] (Extended Data Fig. 1b).

We then tested whether bacteria containing a genomically encoded memory system that requires cell division to function would be able to record information within the beads. Recording information on genomic DNA is advantageous in that DNA is a highly stable information storage medium (turnover time up to weeks in aquatic environments and years in soil[39]), amenable to multiplexing[40], and information can be retrieved from it after cell death. We used our synthetic cellular recorders integrating biological events (SCRIBE) platform[31,41] for targeted in vivo genome editing to record information in encapsulated GMMs. The SCRIBE circuit was designed so that isopropyl-β-D-1-thiogalactopyranoside (IPTG) and aTc controlled the expression of Beta recombinase and the CRISPRi system, respectively; in this design, gene editing of the
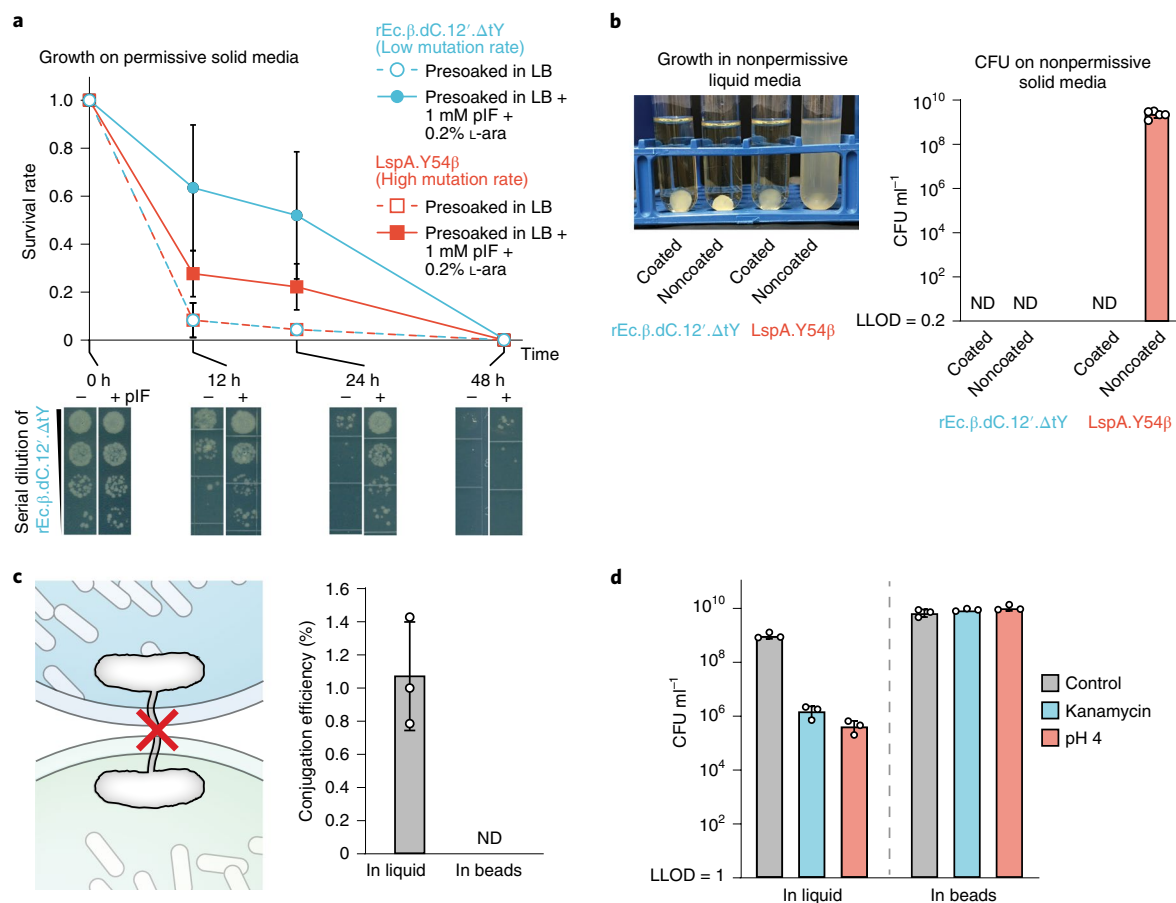
Fig. 4 | Combining chemical and physical containment strategies for optimal biocontainment and protection. a, Comparison of cell survival in beads between two GRO strains with different containment efficiencies. Survival rate calculated by the number of encapsulated GRO in tough hydrogel beads that were presoaked in permissive media (LB + 1 mM pIF + 0.2% L-ara) (closed circles and solid lines) versus encapsulated GRO in tough hydrogel beads that were presoaked in nonpermissive media (LB only) (open circles and dashed lines) before incubation of the beads in LB. Survival rates were calculated by normalizing CFU from samples inside the beads, which were plated on permissive solid media at each time point, to CFU at 0 h. Dilution series of the rEc.β.dC.12′.ΔtY at different incubation time points are shown at the bottom. Samples prepared and measured independently from triplicate, data represent the mean ± 1 s.d. **b**, Left, the escape of GROs into 5 ml of nonpermissive media (LB only) surrounding the coated versus noncoated beads containing the GROs after shaking the tough hydrogel beads at 200 r.p.m. for 3 d. Right, the surrounding media was plated on nonpermissive solid media to obtain CFU counts (ND, not detectable with LLOD = 1 CFU per 5 ml). Samples prepared and measured independently from $n = 5$ beads, data represent the mean ± 1 s.d. **c**, The tough hydrogel shell prevents HGT by direct cell-to-cell conjugation. Conjugation efficiency is calculated as the ratio of recipient strain that acquired the F′ plasmid over the total number of recipient cells in media. Samples prepared in triplicate, data represent the mean ± 1 s.d. **d**, Survival of bacteria after subjecting liquid bacterial cultures or bacteria in tough hydrogel-coated beads to environmental challenges such as antibiotics (30 μg ml⁻¹ kanamycin for 2 h), low pH (pH 4 for 4 h) and untreated controls (LLOD = 200 CFU ml⁻¹). Samples prepared and measured independently from triplicate, data represent the mean ± 1 s.d.

kanR gene records chemical exposure (Fig. 5a, left). We exposed beads containing SCRIBE bacteria to IPTG and aTc over 48 h and found that increasing numbers of bacteria acquired kanamycin resistance over the first 12 h (Fig. 4c, right). The high recombinant frequency (roughly 10%) by 12 h is comparable to results obtained using liquid cultures of nonencapsulated bacteria[31,41], and the plateau in recombination frequency after 12 h corresponds to growth saturation (Supplementary Fig. 4). This DNA-encoded memory is stable and can be retrieved at the end of the testing period and even after cell death without constant monitoring by electronics.

Communication between GMMs in beads can be used to implement computation with higher complexity, division of labor and signal integration/amplification[42,43]. To demonstrate this capability, we showed that different *E. coli* strains contained within beads could communicate with each other via quorum-sensing molecules. An acyl homoserine lactone (AHL) sender strain and an AHL receiver strain were encapsulated in separate beads and incubated

together in 1 ml of Luria-Bertani (LB) medium plus carbenicillin (Fig. 5b, left). On receiving externally added aTc, the sender bead produced AHL, which induced GFP expression in the neighboring receiver bead. The receiver beads exhibited intensified fluorescence (4-, 12- and 21-fold-increase for 1, 2 and 3 sender beads to receiver beads ratio, respectively) as more sender beads were used (Fig. 5b right and Supplementary Fig. 14). These results demonstrate that DEPCOS can enable a modular and distributed strategy for the collective execution of complex tasks based on cell-to-cell communication using multiple beads with different GMMs.

DEPCOS bead can sense contaminants in river water. Finally, to demonstrate that encapsulated bacteria can function in a real-world setting, we used an *E. coli* strain to detect the presence of metal ions in water samples from the Charles River, such as cadmium. Cd²⁺ is a well-known and widespread environmental contaminant that can adversely affect human health[44]. Specifically, we used ZntR, a
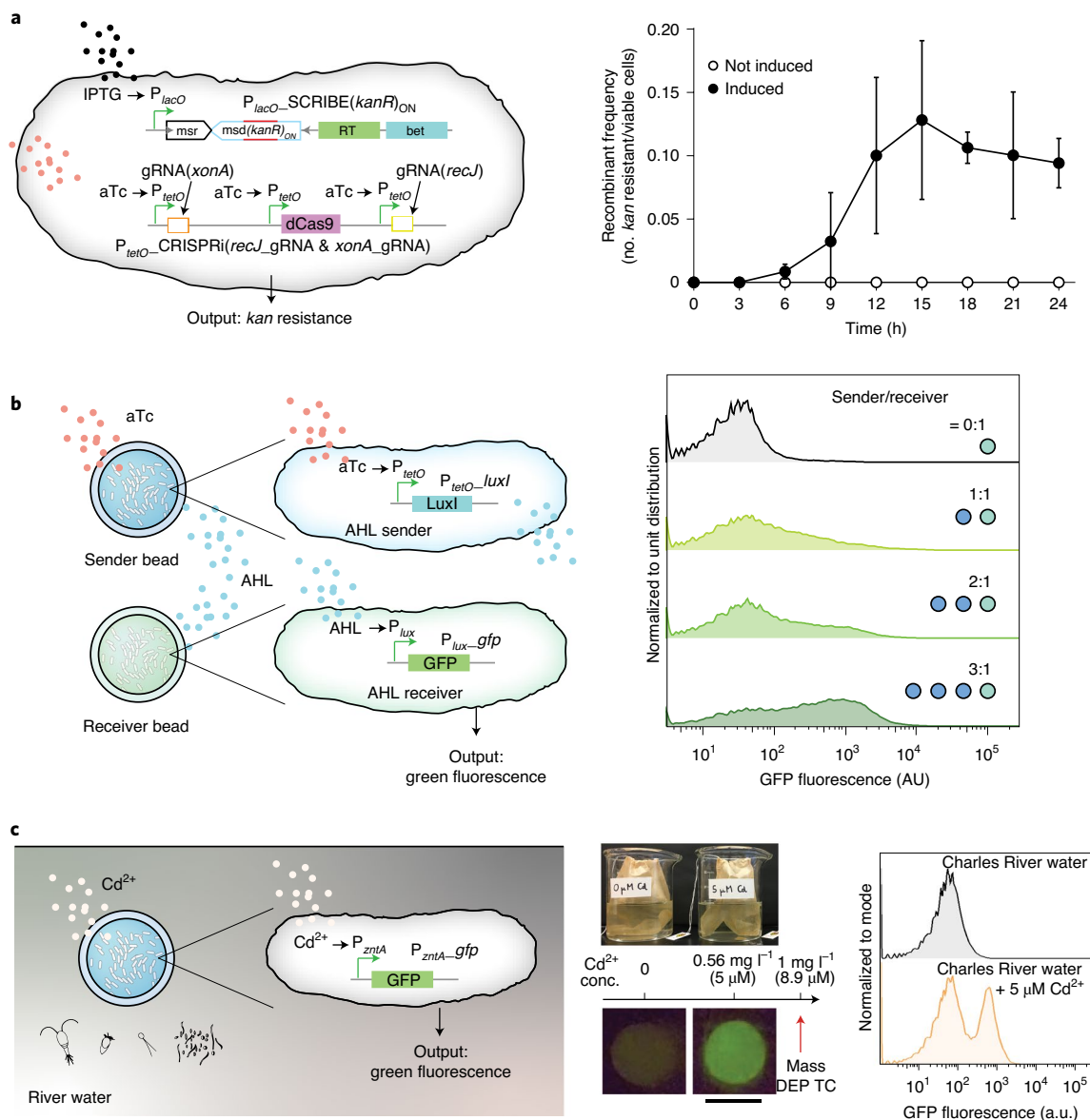
Fig. 5 | Sensing, recording and communication capabilities of encapsulated bacterial cells. a, Left, an improved SCRIBE strain in which CRISPRi is used to knock down cellular exonucleases (encoded by *xonA* and *recJ*) for enhanced genome editing efficiency. Right, recombinant frequencies of beads containing the high-efficiency SCRIBE strain induced for a total of 24 h with or without aTc and IPTG. Samples prepared in triplicate, data represent the mean ± 1 s.d. RT, reverse transcriptase; bet, ssDNA-specific beta recombinase; msr and msd, primer and template for the RT. **b**, Left, an AHL sender strain responds to aTc and produces AHL as an output, which later reaches an AHL receiver strain through diffusion and induces GFP expression. Right, cells retrieved from receiver beads showed various levels of induction corresponding to different AHL sender bead to AHL receiver bead ratios. The data are representative of three independent experiments and normalized to unit distribution (area under the curve). The sender/receiver numbers represent actual number of beads, each contains roughly 10^9 cells. **c**, Left, schematic of GFP expression under the control of a cadmium-inducible promoter. Center, photograph of the heavy-metal sensing experiment setup (top). Tea bags containing five beads each were incubated in beakers containing Charles River water with and without 5 μM CdCl$_2$. The Massachusetts Department of Environmental Protection toxic limit for CdCl$_2$ is 1 mg l^{-1}, corresponding to 8.9 μM. Beads retrieved after 6 h showed green fluorescence (bottom). Right, flow cytometry analysis of encapsulated cells responding to cadmium ions in Charles River water. The flow cytometry panels are representative of samples prepared in triplicate. Data are normalized to mode (peak value). FITC, fluorescein isothiocyanate; AU, arbitrary units. Scale bar, 5 mm.

transcriptional regulator activated by metal ions (Zn^{2+}, Pb^{2+}, Cd^{2+}) that activates the promoter P$_{zntA}$, to express GFP[45]. We characterized the induction of P$_{zntA}$ by Zn^{2+}, Pb^{2+} and Cd^{2+} in liquid cultures of *E. coli* harboring the plasmid pEZ074 (P$_{zntA}$-*gfp* construct) (Fig. 5c, Supplementary Fig. 15a and Supplementary Fig. 16). While encapsulated in hydrogel beads and incubated in LB media for a total of 3 h, cells produced green fluorescence intensities proportional to Cd^{2+} concentrations (Supplementary Fig. 15b and 16).

Next, hydrogel-bacteria beads (presoaked in 4× LB) were incubated in water samples extracted from the Charles River having exogenously added Cd^{2+} (Fig. 5c, center). The hydrogel-bacteria beads were placed in tea bags to facilitate easy deployment and retrieval. Exposure to 5 μM CdCl$_2$ resulted in the emergence of a cell population expressing high levels of GFP (Fig. 5c, right), indicating successful detection of cadmium ions. These results were confirmed visually under blue light: beads exposed to 5 μM CdCl$_2$

exhibited strong green fluorescence (Fig. 5c, center and right and Supplementary Fig. 15c). The high sensitivity of this system to detect $5\,\mu M$ $CdCl_2$ is relevant to real-world use, as it is below the $8.9\,\mu M$ ($1\,mg\,l^{-1}$) standard defined by the Massachusetts Department of Environmental Protection as the maximum concentration of cadmium allowed in waste water. Thus, these results highlight the potential of physically biocontained bacteria to detect toxic levels of heavy metals in environmental settings.

Discussion

Traditionally, GMMs used as environmental sensors are confined in sealed vials into which water samples are manually injected[35,37]. To enable the environmental deployment of GMMs as biosensors and bioremediation devices, new strategies are needed that allow for interactions with the surrounding environment while maintaining containment of GMMs. Tough hydrogel scaffolds provide a highly hydrated environment that can sustain cell growth, protect cells from external stresses and allow small molecules to diffuse between the interior and exterior of the device. Although previous work showed the long-term physical containment of bacteria by core-shell hydrogel microparticles, it did not demonstrate biological activity, robust sensing or high mechanical toughness[19,33,46]. To the best of our knowledge, this is the first report to demonstrate robust physical containment of bacterial cells while still permitting sensing and cell growth, thus overcoming the major limitations for the deployment of GMMs into the real world.

By combining two types of hydrogel into a core-shell structure, we have developed a reliable strategy for the physical containment and protection of microbes that are genetically engineered with heterologous functions. We showed that encapsulated cells could sense environmental and biomedical stimuli, record exogenous signals into genomically encoded memory and communicate with each other via quorum-sensing molecules. Finally, we showed that heavy-metal-sensing bacteria can be incorporated into our hydrogel beads and successfully detect cadmium ions in Charles River water samples.

We anticipate that the DEPCOS containment platform can enable the deployment of microbes engineered with synthetic genetic circuits into real-world scenarios. For example, encapsulated GMMs could be used to safely detect explosives[47] or monitor exposure time to toxic chemicals[48] without potential escape into the wild. In addition, the geometry of DEPCOS could be adapted to meet the design specifications of desired applications, including wearables[23] as well as other living materials and devices[3]. Future work will be focused on automating the manufacturing process to provide precise control over the device size and geometries to accommodate various physical environments and improve the miniaturization and scalability of the platform. We will also explore the incorporation of selective diffusion barriers and extreme pH resistance capabilities into the hydrogels to enable encapsulated microbial populations to survive in harsh environments, such as during transit through the human gastrointestinal tract for detecting disease-relevant biomarkers. Another future challenge lies in devising large-scale standardized tests to determine whether encapsulated organisms can be contained, yet function robustly in harsh real-world scenarios and not just in simulated laboratory settings.

Online content

Any methods, additional references, Nature Research reporting summaries, source data, extended data, supplementary information, acknowledgements, peer review information; details of author contributions and competing interests; and statements of data and code availability are available at https://doi.org/10.1038/s41589-021-00779-6.

References

1. Singh, J. S., Abhilash, P. C., Singh, H. B., Singh, R. P. & Singh, D. P. Genetically engineered bacteria: an emerging tool for environmental remediation and future research perspectives. *Gene* **480**, 1–9 (2011).
2. Farrar, K., Bryant, D. & Cope-Selby, N. Understanding and engineering beneficial plant-microbe interactions: plant growth promotion in energy crops. *Plant Biotechnol. J.* **12**, 1193–1206 (2014).
3. Tang, T.-C. et al. Materials design by synthetic biology. *Nat. Rev. Mater.* https://doi.org/10.1038/s41578-020-00265-w (2020).
4. Dana, G. V., Kuiken, T., Rejeski, D. & Snow, A. A. Synthetic biology: four steps to avoid a synthetic-biology disaster. *Nature* **483**, 29 (2012).
5. Torres, L., Krüger, A., Csibra, E., Gianni, E. & Pinheiro, V. B. Synthetic biology approaches to biological containment: pre-emptively tackling potential risks. *Essays Biochem.* **60**, 393–410 (2016).
6. Epstein, M. M. & Vermeire, T. Scientific opinion on risk assessment of synthetic biology. *Trends Biotechnol.* **34**, 601–603 (2016).
7. Wright, O., Stan, G. B. & Ellis, T. Building-in biosafety for synthetic biology. *Microbiol.* **159**, 1221–1235 (2013).
8. Lee, J. W., Chan, C. T. Y., Slomovic, S. & Collins, J. J. Next-generation biocontainment systems for engineered organisms. *Nat. Chem. Biol.* **14**, 530–537 (2018).
9. Chan, C. T. Y., Lee, J. W., Cameron, D. E., Bashor, C. J. & Collins, J. J. 'Deadman' and 'Passcode' microbial kill switches for bacterial containment. *Nat. Chem. Biol.* **12**, 82–86 (2016).
10. Wright, O., Delmans, M., Stan, G. B. & Ellis, T. GeneGuard: a modular plasmid system designed for biosafety. *ACS Synth. Biol.* **4**, 307–316 (2015).
11. Gallagher, R. R., Patel, J. R., Interiano, A. L., Rovner, A. J. & Isaacs, F. J. Multilayered genetic safeguards limit growth of microorganisms to defined environments. *Nucleic Acids Res.* **43**, 1945–1954 (2015).
12. Rovner, A. J. et al. Recoded organisms engineered to depend on synthetic amino acids. *Nature* **518**, 89–93 (2015).
13. Hoffman, A. S. Hydrogels for biomedical applications. *Adv. Drug Deliv. Rev.* **64**, 18–23 (2012).
14. Choi, M. et al. Light-guiding hydrogels for cell-based sensing and optogenetic synthesis in vivo. *Nat. Photonics* **7**, 987–994 (2013).
15. Anselmo, A. C., McHugh, K. J., Webster, J., Langer, R. & Jaklenec, A. Layer-by-layer encapsulation of probiotics for delivery to the microbiome. *Adv. Mater.* **28**, 9486–9490 (2016).
16. Lee, K. Y. & Mooney, D. J. Alginate: properties and biomedical applications. *Prog. Polym. Sci.* **37**, 106–126 (2012).
17. Kearney, C. J. & Mooney, D. J. Macroscale delivery systems for molecular and cellular payloads. *Nat. Mater.* **12**, 1004–1017 (2013).
18. Billiet, T., Vandenhaute, M., Schelfhout, J., Van Vlierberghe, S. & Dubruel, P. A review of trends and limitations in hydrogel-rapid prototyping for tissue engineering. *Biomaterials* **33**, 6020–6041 (2012).
19. Kim, B. J. et al. Cytoprotective alginate/polydopamine core/shell microcapsules in microbial encapsulation. *Angew. Chem. Int. Ed.* **53**, 14443–14446 (2014).
20. Li, P., Müller, M., Chang, M. W., Frettlöh, M. & Schönherr, H. Encapsulation of autoinducer sensing reporter bacteria in reinforced alginate-based microbeads. *ACS Appl. Mater. Interfaces* **9**, 22331–22331 (2017).
21. Zhang, B. B., Wang, L., Charles, V., Rooke, J. C. & Su, B. L. Robust and biocompatible hybrid matrix with controllable permeability for microalgae encapsulation. *ACS Appl. Mater. Interfaces* **8**, 8939–8946 (2016).
22. Sun, J. Y. et al. Highly stretchable and tough hydrogels. *Nature* **489**, 133–136 (2012).
23. Liu, X. et al. Stretchable living materials and devices with hydrogel-elastomer hybrids hosting programmed cells. *Proc. Natl Acad. Sci. USA* **114**, 2200–2205 (2017).
24. Valade, D., Wong, L. K., Jeon, Y., Jia, Z. & Monteiro, M. J. Polyacrylamide hydrogel membranes with controlled pore sizes. *J. Polym. Sci., Part A: Polym. Chem.* **51**, 129–138 (2013).
25. Atkinson, J. *The Mechanics of Soils and Foundations* 2nd edn (CRC Press, 2007); https://doi.org/10.1201/9781315273549
26. Liu, X. et al. Ingestible hydrogel device. *Nat. Commun.* **10**, 493 (2019).
27. Houghton, L. A. et al. Motor activity of the gastric antrum, pylorus, and duodenum under fasted conditions and after a liquid meal. *Gastroenterology* **94**, 1276–1284 (1988).
28. Zarket, B. C. & Raghavan, S. R. Onion-like multilayered polymer capsules synthesized by a bioinspired inside-out technique. *Nat. Commun.* **8**, 193 (2017).
29. Eun, Y. J., Utada, A. S., Copeland, M. F., Takeuchi, S. & Weibel, D. B. Encapsulating bacteria in agarose microparticles using microfluidics for high-throughput cell analysis and isolation. *ACS Chem. Biol.* **6**, 260–266 (2011).
30. Kong, H. J., Kim, E. S., Huang, Y. C. & Mooney, D. J. Design of biodegradable hydrogel for the local and sustained delivery of angiogenic plasmid DNA. *Pharm. Res.* **25**, 1230–1238 (2008).

31. Farzadfard, F. & Lu, T. K. Genomically encoded analog memory with precise in vivo DNA writing in living cell populations. *Science* **346**, 1256272–1256272 (2014).

32. Golmohamadi, M. & Wilkinson, K. J. Diffusion of ions in a calcium alginate hydrogel-structure is the primary factor controlling diffusion. *Carbohydr. Polym.* **94**, 82–87 (2013).

33. Li, Z. et al. Biofilm-inspired encapsulation of probiotics for the treatment of complex infections. *Adv. Mater.* **30**, e1803925 (2018).

34. Bjerketorp, J., Håkansson, S., Belkin, S. & Jansson, J. K. Advances in preservation methods: keeping biosensor microorganisms alive and active. *Curr. Opin. Biotechnol.* **17**, 43–49 (2006).

35. Roggo, C. & van der Meer, J. R. Miniaturized and integrated whole cell living bacterial sensors in field applicable autonomous devices. *Curr. Opin. Biotechnol.* **45**, 24–33 (2017).

36. Kim, B. C. & Gu, M. B. A bioluminescent sensor for high throughput toxicity classification. *Biosens. Bioelectron.* **18**, 1015–1021 (2003).

37. Cevenini, L., Calabretta, M. M., Tarantino, G., Michelini, E. & Roda, A. Smartphone-interfaced 3D printed toxicity biosensor integrating bioluminescent 'sentinel cells'. *Sens. Actuators, B Chem.* **225**, 249–257 (2016).

38. Mimee, M. et al. An ingestible bacterial-electronic system to monitor gastrointestinal health. *Science* **360**, 915–918 (2018).

39. Pedersen, M. W. et al. Ancient and modern environmental DNA. *Philos. Trans. R. Soc. B Biol. Sci.* **370**, 20130383 (2015).

40. Sheth, R. U. & Wang, H. H. DNA-based memory devices for recording cellular events. *Nat. Rev. Genet.* **19**, 718–732 (2018).

41. Farzadfard, F., Gharaei, N., Citorik, R. J. & Lu, T. K. Efficient retroelement-mediated DNA writing in bacteria. Preprint at *bioRxiv* https://doi.org/10.1101/2020.02.21.958983 (2020).

42. Weiss, R. & Knight, T. F. Jr. in *Cellular Computing* (ed. Amos, M.) 120–121 (Oxford Univ. Press, 2004); https://doi.org/10.1093/oso/9780195155396.003.0012

43. Chen, M. T. & Weiss, R. Artificial cell-cell communication in yeast *Saccharomyces cerevisiae* using signaling elements from *Arabidopsis thaliana*. *Nat. Biotechnol.* **23**, 1551–1555 (2005).

44. Järup, L. & Åkesson, A. Current status of cadmium as an environmental health problem. *Toxicol. Appl. Pharmacol.* **238**, 201–208 (2009).

45. Brocklehurst, K. R. et al. ZntR is a Zn(II)-responsive MerR-like transcriptional regulator of zntA in *Escherichia coli*. *Mol. Microbiol.* **31**, 893–902 (1999).

46. Knierim, C., Greenblatt, C. L., Agarwal, S. & Greiner, A. Blocked bacteria escape by ATRP grafting of a PMMA shell on PVA microparticles. *Macromol. Biosci.* **14**, 537–545 (2014).

47. Belkin, S. et al. Remote detection of buried landmines using a bacterial sensor. *Nat. Biotechnol.* **35**, 308–310 (2017).

48. De Las Heras, A., Carreño, C. A. & De Lorenzo, V. Stable implantation of orthogonal sensor circuits in Gram-negative bacteria for environmental release. *Environ. Microbiol.* **10**, 3305–3316 (2008).

Methods

Bacterial strains and plasmids. A complete listing of bacterial strains and plasmids including their sources can be found in Supplementary Tables 1 and 2. Specifically, pEZ055, pEZ058 and pEZ074 (Supplementary Fig. 17) were constructed on a high copy number plasmid (pZE12) backbone carrying a GFP reporter gene and transformed into DH5αPRO cells. For the aTc-inducible plasmid (pEZ055), the original pZE12 $P_{LlacO-1}$ promoter was replaced by $P_{LtetO-1}$. For the AHL-sensing plasmid (pEZ058), the P_{lux} promoter was PCR amplified and cloned into pZE12 by substituting $P_{LlacO-1}$ promoter via Gibson Assembly. For the heavy-metal-sensing plasmid (pEZ074), the P_{zntA} promoter was PCR amplified from DH5αPRO *E. coli* genomic DNA and cloned into pZE12 by substituting $P_{LlacO-1}$ promoter via Gibson Assembly.

Manufacturing the alginate cores. Here, 5 wt% alginate solution was made by dissolving medium viscosity alginate (Sigma-Aldrich A2033) in MilliQ water followed by autoclaving at 120 °C for 20 min to ensure sterility. A fresh bacterial culture (roughly 10^9 cells per ml in LB plus antibiotics) was then mixed with the alginate solution in a one to one volume ratio to reach a final alginate concentration of 2.5 wt%. This bacteria–alginate premix was loaded into a syringe and disposed onto parafilm to form bead-like droplets. The droplets were solidified by immersing them in 5 wt% CaCl₂ (an ionic crosslinker, Sigma-Aldrich 223506) solution for 15 min.

Coating with tough hydrogel. A precursor solution composed of 2 wt% alginate, 30 wt% acrylamide (Sigma-Aldrich A8887), 0.046 wt% ammonium persulfate (Sigma-Aldrich A3678) and 0.015 wt% *N,N*-methylenebisacrylamide (Sigma-Aldrich 146072) was thoroughly degassed. Before the coating process, the viscous precursor solution was mixed with an accelerator, *N,N,N′,N′*-tetramethylethylenediamine (Sigma-Aldrich T9281, 0.1% times the volume of the precursor solution) to form a fast-curable pregel solution. Alginate cores from the previous section were dipped into the pregel solution to form a tunable thin shell layer of roughly 100–1,000 μm surrounding the core under a nitrogen atmosphere. To stabilize the shell layer, the hydrogel then was immersed in a MES buffer (0.1 M MES and 0.5 M NaCl, pH 6.0) together with crosslinkers and catalysts including 0.00125 wt% 1-ethyl-3-(3-dimethylaminopropyl)carbodiimide, 0.000375 wt% *N*-hydroxysuccinimide and 0.00075 wt% adipic acid dihydrazide to form the covalent bonding between the alginate and polyacrylamide network for 3 h.

Retrieval of bacterial cells. After experiments described in following sections, beads were retrieved from liquid and the tough shell around the alginate core was carefully removed with razor blade and tweezers. The cores were then placed in tubes containing 1 ml of phosphate-buffered solution (PBS) (Research Products International) plus 55 mM sodium citrate (Sigma-Aldrich S4641) and homogenized with 5-mm stainless steel beads on a TissueLyzer II (Qiagen 85300) at 30 Hz for 30 min. To quantify cell density, homogenized samples were serially diluted (10×) and plated on LB plus antibiotics agar plates. CFU were counted after overnight incubation at 37 °C.

Growth of bacteria in beads. All the beads containing *E. coli* cells underwent an outgrowth step after they were taken out of the crosslinking solution to replenish their CFU counts. Each bead was placed in a well on a 24-well plate and incubated in LB plus antibiotics and 20 mM of CaCl₂ at 37 °C. Any beads that showed bacterial growth in the surrounding media were discarded. To quantify the bacterial growth kinetics inside the alginate core, at each time point (every 3 h for a total duration of 24 h, Supplementary Fig. 4), cells were retrieved from beads and plated on LB plus antibiotics agar plates for CFU counting.

Comparison with alginate and agarose shell. Alginate cores containing EZ074 cells were prepared as described previously. For coating with alginate shell[33], alginate cores were dipped in 2.5 wt% alginate solution and crosslinked in 0.1 M CaCl₂ for 30 min. For coating with agarose shell[29], alginate cores were covered by 2 wt% agarose solution (roughly 40 °C) and left to solidify for 30 min. Coated beads were then incubated in 1 ml of LB plus antibiotics and shaken at 200 r.p.m. for 12 h at 37 °C.

Swelling test. Hydrogel beads containing EZ074 cells were incubated in PBS plus 20 mM of CaCl₂ at 37 °C for 14 d. At given time points, the beads were retrieved and weighted (normalized to D0) using an electronic scale. Day 0 was defined as 12 h postmanufacturing of the beads.

Compression test. The compression of hydrogel beads was carried out using a mechanical testing machine (Z2.5 with testXpert Ill Vl.11, Zwick/Roell) with a 20-N load cell. The samples were compressed in air or in PBS plus 20 mM of CaCl₂ by two rigid flat substrates at a loading speed of 2 mm min⁻¹. As the beads will be immersed in liquid in all practical applications, the mechanical properties (force and displacement) in air were determined in the swollen state. This was carried out by keeping the bead immerged in PBS plus 20 mM of CaCl₂ up until the measurement. The approximate engineering stress is defined as:

$$\frac{P}{\pi r_0^2}$$

where r_0 and P are the initial radius of the bead and the magnitude of the compressive load, respectively[26,49]. After testing, beads were incubated in LB overnight and the surrounding media were plated to detect potential cell leakage from compression.

Controlling GRO lifespan. GROs (rEc.β.dC.12′.ΔtY and LspA.Y54β) were grown in LB plus 1 mM pIF (Sigma-Aldrich I8757), 0.02% ʟ-ara and carbenicillin at 30 °C overnight[12], washed twice with PBS to remove pIF and ʟ-ara, and encapsulated in hydrogel beads. GRO beads were then incubated in LB plus carbenicillin with or without 1 mM pIF at 4 °C overnight to allow pIF infusion. At $t = 0$, beads were placed in 50 ml of LB medium and incubated at 30 °C for 12, 24 and 48 h. Cells were retrieved at given time points and plated on LB plus carbenicillin with 1 mM pIF and 0.02% ʟ-ara agar plates for CFU counting. Survival rates were calculated by normalizing CFU counts to $t = 0$.

Detecting GRO escape. GROs (rEc.β.dC.12′.ΔtY and LspA.Y54β) were grown in LB plus 1 mM pIF, 0.02% ʟ-ara and carbenicillin at 30 °C overnight, washed twice with PBS to remove pIF and ʟ-ara, and encapsulated in alginate beads with or without the tough hydrogel coating. The beads were then incubated in 5 ml of LB plus carbenicillin at 30 °C with 200 r.p.m. shaking for 3 d. Media from each tube was plated on LB plus carbenicillin plates for CFU counts.

Environmental insult experiments. For antibiotics and acidic condition treatments, beads containing EZ074 cells were incubated in 1 ml of LB plus carbenicillin at 37 °C for 12 to bring cell densities in the different beads to a similar level (roughly 10^9 per bead). At $t = 0$, culture media was switched to LB plus 30 μg ml⁻¹ kanamycin and LB at pH 4, respectively. At the end of the experiments, beads were retrieved from liquid media and cells were gathered for CFU counting.

Microscopy of hydrogel beads. Hydrogel beads containing EZ074 cells postoutgrowth were incubated in LB at pH 4 and shaken at 120 r.p.m. at 37 °C for 4 h. At the end of treatment, the alginate cores of the beads were retrieved and washed in PBS twice. The cores were cut in half with a razor blade and stained using the Live/Dead BacLight Bacterial Viability Kit for microscopy and quantitative assays (Thermo Fisher Scientific L7012). Microscopy was performed using a confocal microscope (Leica SP 8 with LAS X 3.1.5.16308) with excitation wavelength at 495 nm and emission wavelength at 515 nm for living cells, and excitation wavelength at 495 nm and emission wavelength at 635 nm for dead cells. Z stack was performed at a fixed step size of 17 μm.

Bacterial conjugation. The F′ plasmid (containing chloramphenicol resistance) donor strain CJ236 was encapsulated in beads and underwent overnight outgrowth in LB without antibiotics. The donor beads were placed in 2 ml of LB and cocultured with recipient strain rcF453 (with streptomycin resistance). After 24 h of incubation at 37 °C (shaking at 100 r.p.m.), the surrounding media was plated on LB plus streptomycin (Sm, 25 μg ml⁻¹) and LB plus streptomycin (25 μg ml⁻¹) and chloramphenicol (Cm, 12.5 μg ml⁻¹). The conjugation efficiency was calculated as:

$$\frac{\text{CFU on LB + Sm + Cm}}{\text{CFU on LB + Sm}}$$

DNA escape test. A linear DNA fragment encoding a GFP transcriptional unit (roughly 1,000 bp) was amplified using PCR and encapsulated in the hydrogel beads at 3×10^9 copy per μl. Soluble DNA in the surrounding media after 72-h incubation was quantified using qPCR (Roche LightCycler 96 with LightCycler 96 Instrument Software vi.1) with an optimized amplicon (314 bp). A standard curve was constructed using a serial dilution (10×) of the same fragment.

Small molecule diffusion assay. Two fluorescent dyes, rhodamine B and fluorescein, were used as surrogates for small molecule diffusion assay. Coated beads were soaked in dye solutions for various time periods, weighted and transferred into 2 ml of PBS and incubated in dark for 24 h. The fluorescence of the PBS at equilibrium was measured (494/521 and 540/625 nm with a Synergy H1 Hybrid Multi-Mode Reader with Gens Vl.11.5, BioTek Instruments), calibrated by the total weight of PBS plus bead and normalized to the saturated maximum incubation period in dyes (24 h).

aTc induction in beads. Beads containing EZ055 were incubated in LB plus carbenicillin and 200 ng ml⁻¹ aTc at 37 °C for 8 h. The bead was then retrieved and sliced with a sharp razor blade at thickness of roughly 0.5 mm. The sliced sample was then imaged with a Zeiss LSM 700 confocal microscope with excitation wavelength at 488 nm and emission wavelength at 515 nm. To test inducibility after long-term storage, beads were kept at 4 °C over the course of 30 d. At each time point, beads were retrieved and induced in LB plus carbenicillin and 200 ng ml⁻¹

aTc at 37 °C for 8 h. Fluorescence profiles were characterized using a Synergy H1 Hybrid Multi-Mode Reader (488 nm excitation, 530/30 detection).

Heme sensing in beads. Defibrinated horse blood (Hemostat Laboratories DHB030) was used as the source of blood and was lysed by first diluting 1:10 in simulated gastric fluid (SGF) (0.2% NaCl, 0.32% pepsin, 84 mM HCl, pH 1.2) to release heme. This stock solution was diluted to 300 ppm in PBS right before experiments. Beads were placed in PBS or PBS + blood for 8 h at 37 °C. Cells were retrieved and measured for luminescence using a Synergy H1 plate reader. The relative luminescence units were normalized by CFU (measured through plating). Luminescence images of intact beads were acquired using a ChemiDoc Touch Imaging System (Bio-Rad).

Memory of chemical exposure (SCRIBE) in beads. An higher efficiency version of SCRIBE was used in this study[31,41]. The SCRIBE strain was encapsulated in tough hydrogel beads and incubated in LB media with carbenicillin (100 μg ml⁻¹), chloramphenicol (25 μg ml⁻¹), aTc (100 ng ml⁻¹) and IPTG (1 mM) at 37 °C. A control group was incubated using the same conditions but without the inducers (aTc and IPTG). At given time points, cells were retrieved from the beads and plated on LB plus kanamycin (50 μg ml⁻¹) agar plates as well as LB plus carbenicillin and chloramphenicol agar plates. The recombinant frequency was calculated by dividing the colony count on the LB plus kanamycin plate (*kan*-resistant cells) by the colony count on the LB plus carbenicillin and chloramphenicol plate (total viable cells).

Quorum sensing between beads. Beads containing the AHL sender strain (AYC261) and AHL receiver strain (EZ058) were placed in 1 ml of LB plus 250 ng ml⁻¹ aTc in a 12-well plate at specific ratios (sender/receiver ratios, 0/1, 1/1, 2/1 and 3/1). After 24 h of incubation at 37 °C, we retrieved and diluted AHL receiver cells 1:20 into PBS (Research Products International) and ran them on a BD-FACS LSRFortessa-HTS cell analyzer (BD Biosciences) with BD FACSDiva 8.0.1. We measured at least 20,000 cells for each sample and consistently gated by forward scatter and side scatter for all cells in an experiment. GFP intensity was measured on the fluorescein isothiocyanate channel (488-nm excitation laser, 530/30 detection filter). Data from flow cytometry are normalized to unit distribution (normalized to area under the curve). Cells were gated using log forward scatter area by log side scatter area, followed by gating on log forward scatter height by log side scatter height and subsequent gating on log forward scatter width by log side scatter width, as exemplified in Supplementary Fig. 18.

Heavy-metal sensing. To test inducibility of the Zn/Pb/Cd sensing strain (EZ074) in liquid, cells were grown overnight and diluted 200× in fresh LB plus 300 μM ZnCl₂, 100 μM Pb(NO₃)₂ and 10 μM CdCl₂, respectively, on a 96-well plate. After 3 h of incubation at 37 °C, we retrieved bacterial cells and analyzed their GFP profile with flow cytometry. To build the dose-response curves for Cd²⁺ induction, overnight culture of EZ074 was diluted 200× in fresh LB plus antibiotics and induced with different concentrations of CdCl₂. The GFP expression profiles were measured using a Synergy H1 Hybrid Multi-Mode Reader and normalized to their optical density (OD_{600}) values. For testing inducibility in beads, EZ074 was encapsulated in tough hydrogel bead and incubated overnight in LB media with antibiotics at 4 °C. Before the experiment, beads were incubated at 37 °C for 12 h for bacterial cell outgrowth. Hydrogel beads were then placed in fresh LB medium with carbenicillin and corresponding metal ions at given concentrations and incubated at 37 °C for 3 h. Bacterial cells were retrieved and analyzed with flow cytometry. Data from flow cytometry are normalized to mode (normalized to peak value), which allows the visualization of differences in relative percentages of cell populations of interest.

Metal sensing in Charles River water. Beads containing EZ074 were incubated in 4× LB media at 4 °C overnight to reach equilibrium. At $t = 0$, beads were placed in tea bags and transferred to beakers containing 100 ml of fresh Charles River water with or without 5 mM CdCl₂. After 6 h of incubation at room temperature, cells were retrieved and analyzed with flow cytometry. Data from flow cytometry were normalized to mode.

Data analysis. All data were processed and plotted using GraphPad Prism for Windows 64-bit v.8.4.3 (686) and Microsoft Excel for Mac v.16.16.17.

Reporting Summary. Further information on research design is available in the Nature Research Reporting Summary linked to this article.

Data availability
Data supporting this study are presented in the main text and Supplementary Information, and are available from the corresponding authors upon request. Source data are provided with this paper.

References
49. Tomović, N. S., Trifković, K. T., Rakin, M. P., Rakin, M. B. & Bugarski, B. M. Influence of compression speed and deformation percentage on mechanical properties of calcium alginate particles. *Chem. Ind. Chem. Eng. Q.* **21**, 411–417 (2015).

Acknowledgements

Author contributions
T.-C.T., E.T., X.L., X.Z. and T.K.L. conceived and designed the research. T.-C.T., E.T., X.L. and H.Y. performed encapsulation and mechanical testing experiments. T.-C.T. and E.T. performed genetic circuit experiments. T.-C.T., E.T. and A.J.R. performed GRO experiments. T.-C.T. and E.T. performed river water experiments. T.-C.T., E.T., X.L., K.Y., A.J.R., C.F.-N., F.J.I., X.Z. and T.K.L. analyzed the data and wrote the manuscript.

Competing interests

Additional information

Extended Data Fig. 1 | Responses of encapsulated bacterial cells to external stimuli. (a) Left: Schematic of GFP expression under the control of an aTc-inducible promoter. Center: Flow cytometry analysis of GFP expression in liquid culture and in hydrogel beads. Samples prepared in triplicate, data represent the mean ±1 s.d. based on analyses of 30000 events. The percentage data were calculated by dividing the numbers of GFP ON cells with the total cell counts. The fold-change data were derived from the mean of fluorescence. Right: Confocal microscopy images of beads encapsulating the aTc-sensing *E. coli* strain with and without 200 ng/mL aTc. **(b)** Left: A heme sensing strain which sense heme and generate bioluminescence as an output. The heme released from blood is transported into the cell by ChuA. Middle: Cells retrieved from beads showed a significant increase in luciferase activity. Right: The resulting bioluminescence can be detected with high sensitivity from intact beads. Samples prepared in triplicate, data represent the mean ±1 s.d.

Corresponding author(s): Tzu-Chieh Tang
Xuanhe Zhao
Timothy K. Lu

Last updated by author(s): Jan 27, 2021

Reporting Summary

Nature Research wishes to improve the reproducibility of the work that we publish. This form provides structure for consistency and transparency in reporting. For further information on Nature Research policies, see our Editorial Policies and the Editorial Policy Checklist.

Statistics

For all statistical analyses, confirm that the following items are present in the figure legend, table legend, main text, or Methods section.

n/a	Confirmed	
☐	☒	The exact sample size (*n*) for each experimental group/condition, given as a discrete number and unit of measurement
☐	☒	A statement on whether measurements were taken from distinct samples or whether the same sample was measured repeatedly
☐	☒	The statistical test(s) used AND whether they are one- or two-sided *Only common tests should be described solely by name; describe more complex techniques in the Methods section.*
☒	☐	A description of all covariates tested
☒	☐	A description of any assumptions or corrections, such as tests of normality and adjustment for multiple comparisons
☐	☒	A full description of the statistical parameters including central tendency (e.g. means) or other basic estimates (e.g. regression coefficient) AND variation (e.g. standard deviation) or associated estimates of uncertainty (e.g. confidence intervals)
☐	☒	For null hypothesis testing, the test statistic (e.g. *F*, *t*, *r*) with confidence intervals, effect sizes, degrees of freedom and *P* value noted *Give P values as exact values whenever suitable.*
☒	☐	For Bayesian analysis, information on the choice of priors and Markov chain Monte Carlo settings
☒	☐	For hierarchical and complex designs, identification of the appropriate level for tests and full reporting of outcomes
☒	☐	Estimates of effect sizes (e.g. Cohen's *d*, Pearson's *r*), indicating how they were calculated

Our web collection on statistics for biologists contains articles on many of the points above.

Software and code

Policy information about availability of computer code

Data collection	Tensile test data were collected using a Zwick mechanical tester (Z2.5, Roell) with testXpert III Vl.11. Fluorescence and absorbance data were collected using a plate reader (Synergy Hl, BioTek) with Gens Vl.11.5. qPCR data were collected using a Roche LightCycler 96 with LightCycler® 96 Instrument Software Vl.1. Flow cytometry data were collected and analyzed using a BD-FACS LSRFortessa-HTS cell analyzer with BD FACSDiva 8.0.1. Microscopy data were collected using a Leica SP8 microscope with LAS X 3.1.5.16308
Data analysis	Microsoft Excel for Mac V16.16.17. Graph Pad Prism for Windows 64-bit V8.4.3 (686)

For manuscripts utilizing custom algorithms or software that are central to the research but not yet described in published literature, software must be made available to editors and reviewers. We strongly encourage code deposition in a community repository (e.g. GitHub). See the Nature Research guidelines for submitting code & software for further information.

Data

Policy information about availability of data

All manuscripts must include a data availability statement. This statement should provide the following information, where applicable:

- Accession codes, unique identifiers, or web links for publicly available datasets
- A list of figures that have associated raw data
- A description of any restrictions on data availability

Data supporting this study are presented in the main text and Supplementary Information, and are available from the corresponding author upon request. Source data are provided with this paper.

Field-specific reporting

Please select the one below that is the best fit for your research. If you are not sure, read the appropriate sections before making your selection.

☒ Life sciences   ☐ Behavioural & social sciences   ☐ Ecological, evolutionary & environmental sciences

For a reference copy of the document with all sections, see nature.com/documents/nr-reporting-summary-flat.pdf

Life sciences study design

All studies must disclose on these points even when the disclosure is negative.

Sample size	No sample size calculation was performed. All experiments were performed independently with at least three replicates, which is standard in our field, and were determined by accounting for batch variability. The number of independent experiments and biological replicates are described in each figure or its legend.
Data exclusions	No data were excluded from the analyses.
Replication	All measurements were replicated successfully at least three times. Biological triplicates were performed independently. Material characterization was performed at the same time.
Randomization	No random sample allocation methods were performed because genetically identical samples were used.
Blinding	Blinding was not applied to the performed studies, as no participants groups were involved.

Reporting for specific materials, systems and methods

We require information from authors about some types of materials, experimental systems and methods used in many studies. Here, indicate whether each material, system or method listed is relevant to your study. If you are not sure if a list item applies to your research, read the appropriate section before selecting a response.

Materials & experimental systems

n/a	Involved in the study
☒	☐ Antibodies
☒	☐ Eukaryotic cell lines
☒	☐ Palaeontology and archaeology
☒	☐ Animals and other organisms
☒	☐ Human research participants
☒	☐ Clinical data
☒	☐ Dual use research of concern

Methods

n/a	Involved in the study
☒	☐ ChIP-seq
☐	☒ Flow cytometry
☒	☐ MRI-based neuroimaging

Flow Cytometry

Plots

Confirm that:

☒ The axis labels state the marker and fluorochrome used (e.g. CD4-FITC).

☒ The axis scales are clearly visible. Include numbers along axes only for bottom left plot of group (a 'group' is an analysis of identical markers).

☒ All plots are contour plots with outliers or pseudocolor plots.

☒ A numerical value for number of cells or percentage (with statistics) is provided.

Methodology

Sample preparation	Samples were diluted in PBS and filtered prior measurement.
Instrument	BD-FACS LSRFortessa-HTS cell analyzer
Software	BD FACSDiva 8.0.1
Cell population abundance	10,000-30,000 cells (after gating) from each sample. An example is provided in Supplementary Fig. 18.

Gating strategy

Cells were gated using log forward scatter area (FSC-A) by log side scatter area (SSC-A), followed by gating on log forward scatter height (FSC-H) by log side scatter height (SSC-H), and subsequent gating on log forward scatter width (FSC-W) by log side scatter width (SSC-W). An example is provided in Supplementary Fig. 18.

☒ Tick this box to confirm that a figure exemplifying the gating strategy is provided in the Supplementary Information.

Supplementary information

Hydrogel-based biocontainment of bacteria for continuous sensing and computation

In the format provided by the
authors and unedited

Supplementary Materials

Hydrogel-Based Biocontainment of Bacteria for Continuous Sensing and Computation

Tzu-Chieh Tang[1,2,3,17,*], Eléonore Tham[1,4,17], Xinyue Liu[5,17], Kevin Yehl[1,2,13], Alexis J. Rovner[6,7], Hyunwoo Yuk[5], Cesar de la Fuente-Nunez[1,2,14,15,16], Farren J. Isaacs[8,9,10], Xuanhe Zhao[5,11,*], Timothy K. Lu[1,2,12,*]

[1]Synthetic Biology Group, Research Laboratory of Electronics, Massachusetts Institute of Technology, Cambridge, MA 02139, USA.
[2]Department of Biological Engineering, Massachusetts Institute of Technology, Cambridge, MA 02139, USA.
[3]The Mediated Matter Group, Media Lab, Massachusetts Institute of Technology, Cambridge, MA 02139, USA
[4]Department of Materials Science and Engineering, Massachusetts Institute of Technology, Cambridge, MA 02139, USA.
[5]Department of Mechanical Engineering, Massachusetts Institute of Technology, Cambridge, MA 02139, USA.
[6]Wyss Institute for Biologically Inspired Engineering, Boston, MA 02115, USA.
[7]Department of Genetics, Harvard Medical School, Harvard University, Boston, MA 02115, USA.
[8]Department of Molecular, Cellular and Developmental Biology, Yale University, New Haven, CT 06520, USA.
[9]Systems Biology Institute, Yale University, West Haven, CT 06516, USA.
[10]Department of Biomedical Engineering, Yale University, New Haven, CT 06520, USA
[11]Department of Civil and Environmental Engineering, Massachusetts Institute of Technology, Cambridge, MA 02139, USA
[12]Department of Electrical Engineering and Computer Science, Massachusetts Institute of Technology, Cambridge, MA 02139, USA.
[13]Present address: Department of Chemistry and Biochemistry, Miami University, Oxford, OH 45056, USA.
[14]Present address: Machine Biology Group, Departments of Psychiatry and Microbiology, Institute for Biomedical Informatics, Institute for Translational Medicine and Therapeutics, Perelman School of Medicine, University of Pennsylvania, Philadelphia, PA 19104, USA.
[15]Present address: Departments of Bioengineering and Chemical and Biomolecular Engineering, School of Engineering and Applied Science, University of Pennsylvania, Philadelphia, PA 19104, USA.
[16]Present address: Penn Institute for Computational Science, University of Pennsylvania, Philadelphia, PA 19104, USA.

[17]T.-C.T., E.T., and X.L. contributed equally to this work.

*Correspondence and requests of materials should be addressed to T.-C.T. (zijaytang@gmail.com), X.Z. (zhaox@mit.edu), and T.K.L. (timlu@mit.edu).

Supplementary Tables & Figures

Supplementary Table 1 | List of bacterial strains used in this study

Name	Strain code	Construction method	Genotype	Used in
GRO, pIF auxotroph strain	rEc.β.dC.12'.ΔtY	Ref[1]	MG1655	Fig. 4
GRO, pIF auxotroph strain	LspA.Y54β	Ref[1]	MG1655	Fig. 4
aTc sensing strain	EZ055	DH5αPRO cells transformed with the pEZ055 plasmid	DH5αPRO	Fig. 3 Fig. 5
F' plasmid donor strain	CJ236	Acquired from NEB	K12	Fig. 4
F' plasmid recipient strain	rcF453	Spontaneous resistant mutants generated from plating and re-streaking MG1655 on LB+Sm plate	MG1655	Fig. 4
Zn/Pb/Cd sensing strain	EZ074	DH5αPRO cells transformed with the pEZ074 plasmid	DH5αPRO	Fig. 5
SCRIBE $kanR_{OFF}$ reporter strain	F144	Ref[2]	DH5αPRO $galK::kanR_{W28TAA, A29TAG}$	Fig. 5
AHL sender strain	AYC261	Ref[3]	DH5αPRO	Fig. 5
AHL receiver strain	EZ058	DH5αPRO cells transformed with the pEZ058 plasmid	DH5αPRO	Fig. 5
Heme sensing strain	mm1560	Ref[4]	Nissle 1917	Fig. 5

Supplementary Table 2 | List of plasmids used in this study

Name	Plasmid code	Construction method	Used in
$P_{LtetO-1}$_*gfp*	pEZ055	See Methods and Supplementary Fig. 17	Fig. 5
P_{lux}_*gfp*	pEZ058	See Methods and Supplementary Fig. 17	Fig. 5
P_{zntA}_*gfp*	pEZ074	See Methods and Supplementary Fig. 17	Fig. 5
P_{lacO}_SCRIBE(*kanR*)on	F944	Ref[2]	Fig. 5
P_{TetO}_CRISPRi(*recJ*_gRNA & *xonA* gRNA)	F1156	Ref[5]	Fig. 5
P_{TetO}_*LuxI*	AYC261	Ref[3]	Fig. 5

Supplementary Fig. 1

Supplementary Fig. 1 | Alginate cores in various geometries. The alginate core used to encapsulate cells can be shaped into spheres with different radii through extrusion with syringes and needles on parafilm followed by crosslinking in calcium chloride solution. Alginate thread was produced by direct extrusion in calcium chloride solution. Disk, cube, and cylinder-like structures can be achieved through cutting.
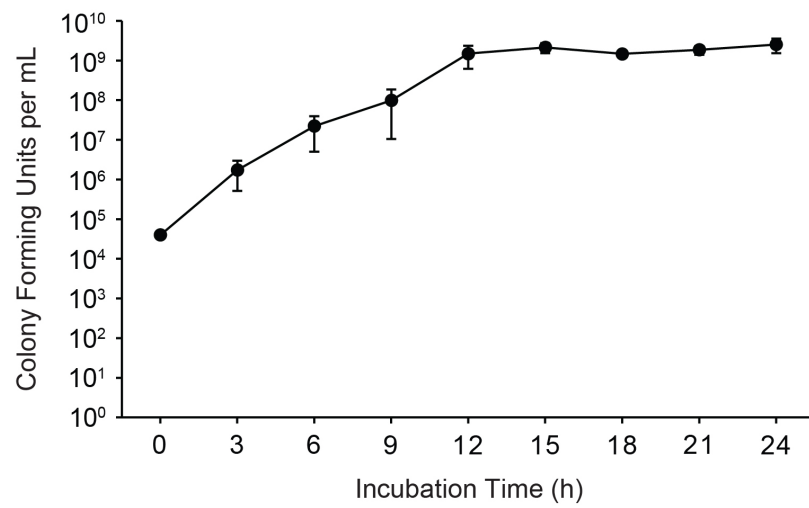
Supplementary Fig. 2
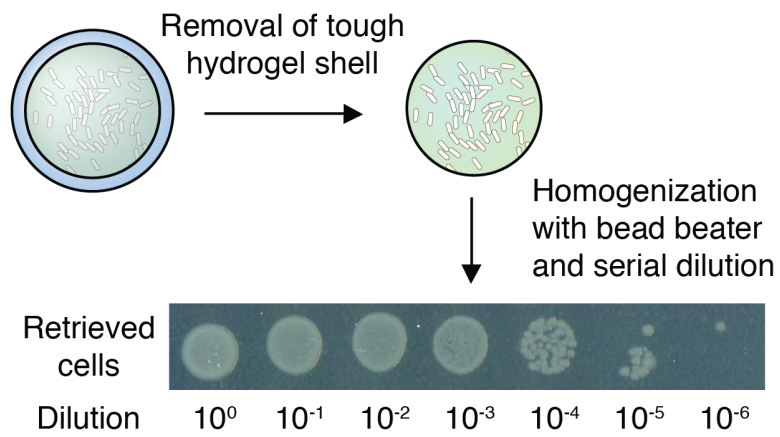
Supplementary Fig. 2 | Retrieving encapsulated cells. Retrieval of live cells from the beads immediately before the cross-linking step. Retrieval was performed through removal of the tough shell followed by homogenization and showed nearly full recovery ($\sim 10^9$ CFU per mL).

Supplementary Fig. 3

a

b
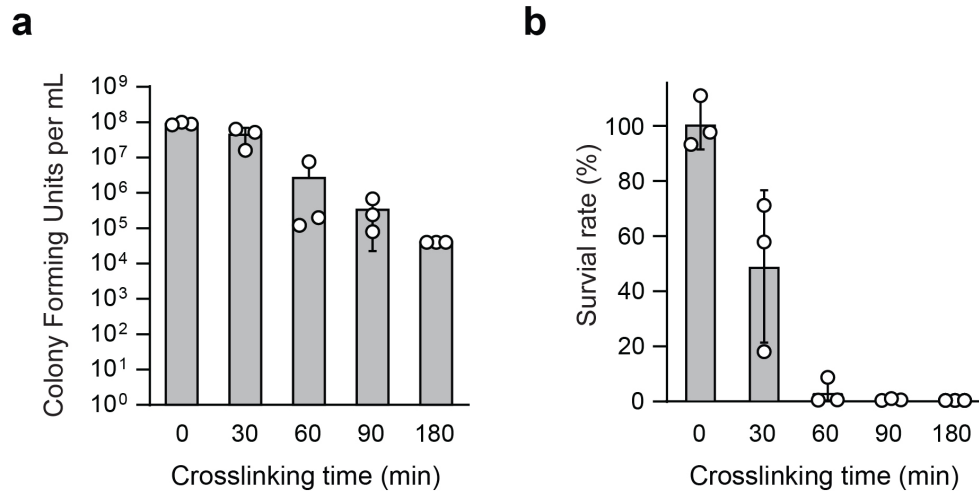
Supplementary Fig. 3 | Toxicity of the chemical crosslinkers. (a) CFU counts and **(b)** survival rates for cells retrieved from hydrogel beads after incubating in the crosslinking solution for different lengths of time. Samples prepared in triplicate, data represent the mean ±1 SD.

Supplementary Fig. 4

Supplementary Fig. 4 | Growth curve of bacteria in hydrogel beads. Cell encapsulated in beads were incubated in LB medium and retrieved at given time points to measure growth over 24 hours. Samples prepared in triplicate, data represent the mean ±1 SD.

Supplementary Fig. 5

Biocontainment of coated beads
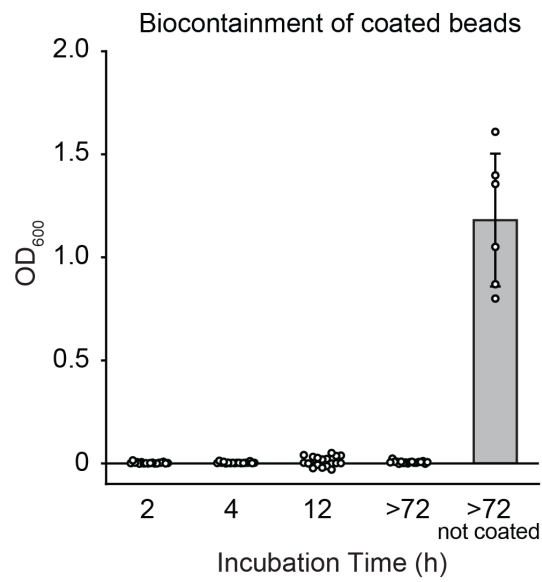
Supplementary Fig. 5 | Long-term physical containment. Optical density at 600 nm (OD_{600}) measurement demonstrating that the media surrounding coated beads showed no bacterial growth after 72 hours. Samples prepared in n = 18 coated beads for h = 2, 4, 12, and >72, and n = 6 beads that are not coated. Data represent the mean ±1 SD.
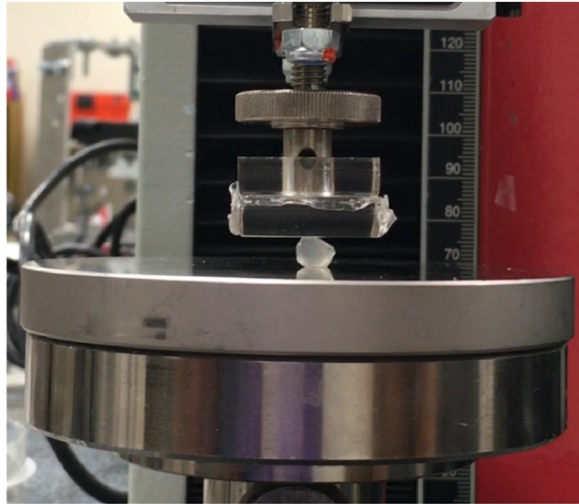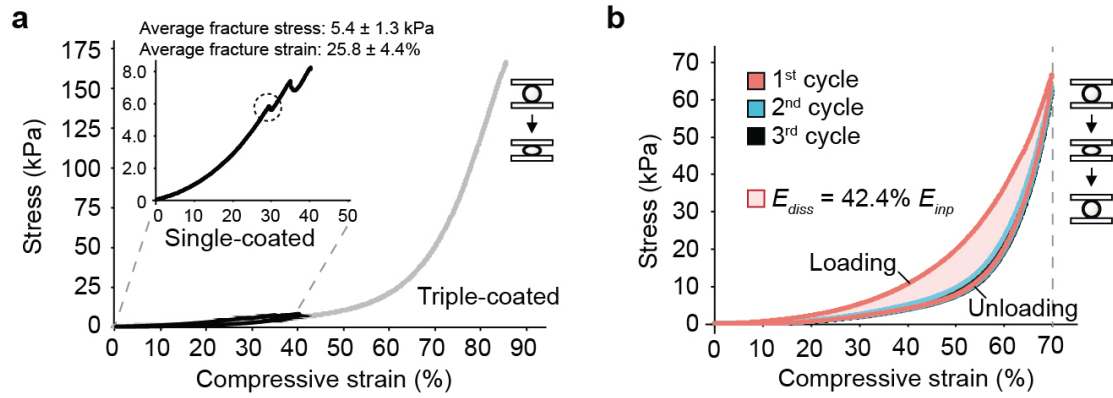
Supplementary Fig. 6

a

b
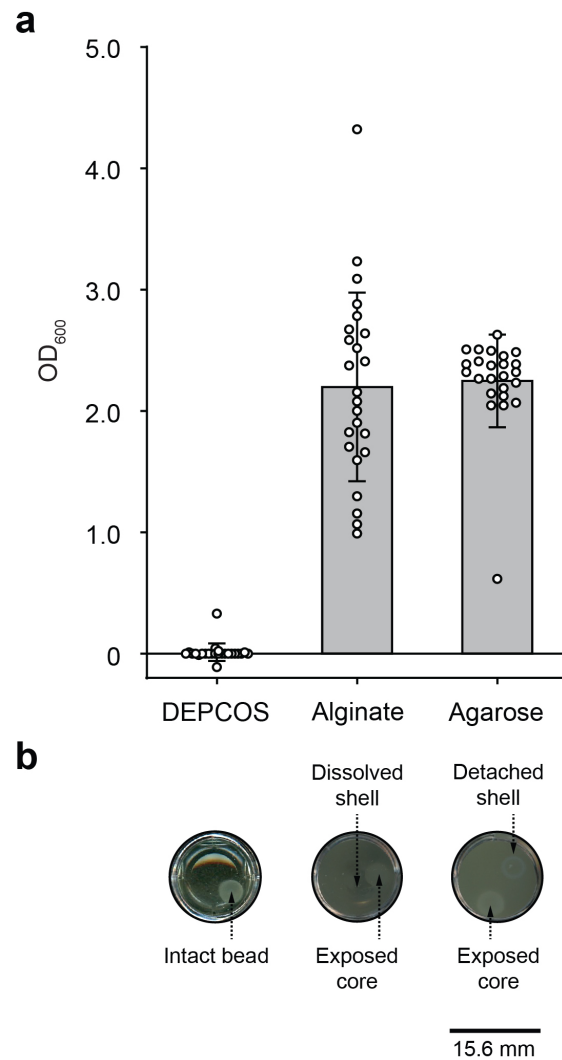
Supplementary Fig. 6 | Physical containment under prolonged shaking. (a) OD_{600} measurement demonstrating the bacterial growth in the media surrounding the beads after 12 hours of shaking at 200 rpm. Samples prepared in n = 24 beads, data represent the mean ±1 SD. **(b)** Representative images of the beads and their surrounding media after shaking. The DEPCOS beads (left) remained intact and showed no signs of cell leakage (clear media). The shell of the alginate-coated beads (center) was dissolved after prolonged shaking and could not stop the core from exposing. Similarly, the shell of the agarose-coated beads broke and detached from the core, leaving it exposed and causing cell escape.
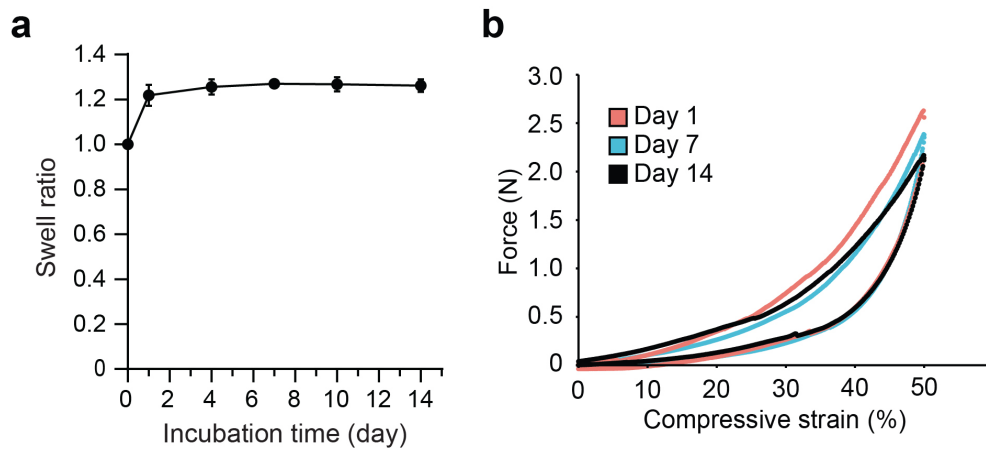
Supplementary Fig. 7

Supplementary Fig. 7 | Compression test setup with Zwick mechanical tester. A fully-hydrated hydrogel bead (r = 3 mm) was placed between sterile surfaces and submitted to compressions.
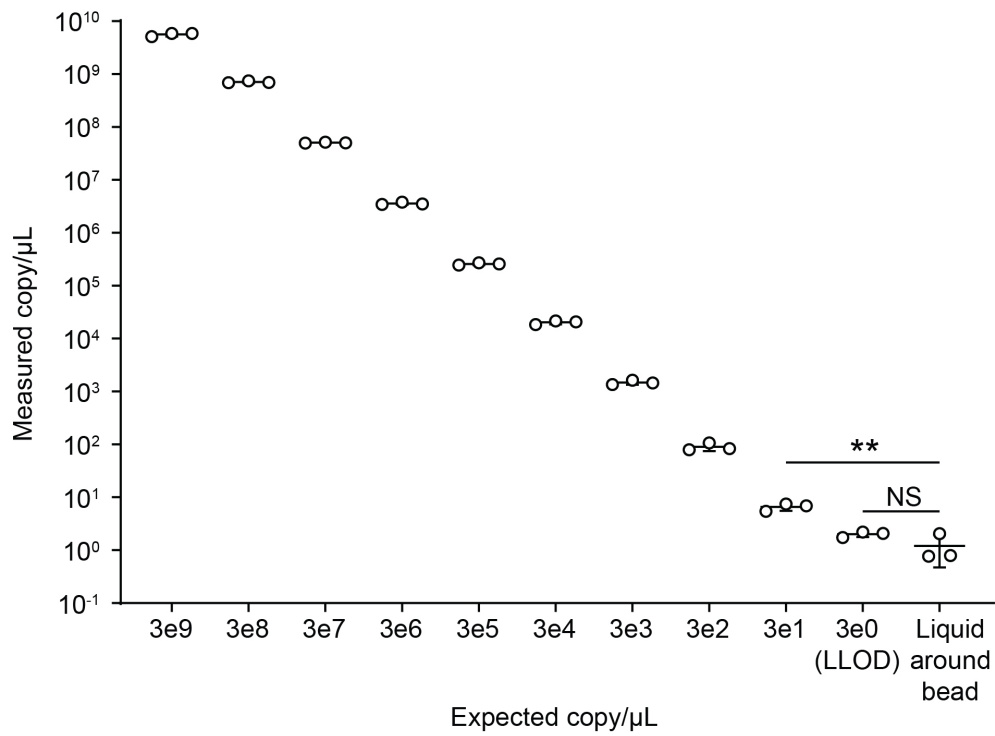
Supplementary Fig. 8

a

Average fracture stress: 5.4 ± 1.3 kPa
Average fracture strain: 25.8 ± 4.4%

Single-coated

Triple-coated

Stress (kPa)

Compressive strain (%)

b

- 1st cycle
- 2nd cycle
- 3rd cycle

E_{diss} = 42.4% E_{inp}

Loading

Unloading

Stress (kPa)

Compressive strain (%)

Supplementary Fig. 8 | Effective stress-strain profiles of the hydrogel beads under compression. (a) Effective stress-strain curves of single- and triple-coated beads. Samples prepared in n = 14 beads. **(b)** Effective stress-strain curves of cyclic compression of triple-coated beads. Effective stress-strain curves were converted from force-displacement curves using the initial dimensions of the beads before compressions[6,7]. Samples prepared in triplicate.
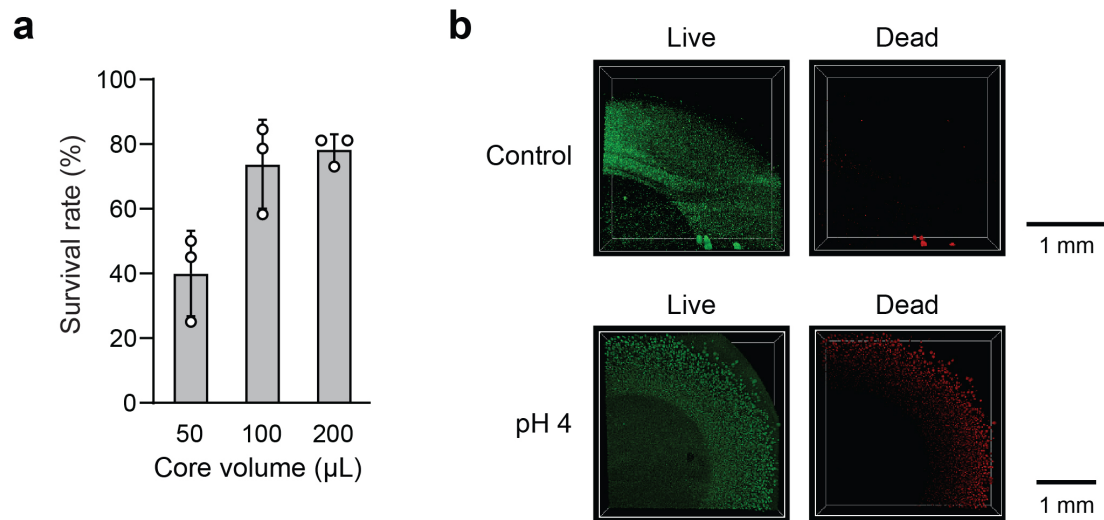
Supplementary Fig. 9

a

b

Supplementary Fig. 9 | Swelling and mechanical properties of the hydrogel beads after prolonged incubation. (a) The swelling behavior of beads over the course of 14 days. Samples prepared in n = 10 beads, data represent the mean ±1 SD. **(b**) Typical force-displacement curves of single-layer coated bead (r = 3 mm) on day 1, 7, and 14 of incubation.
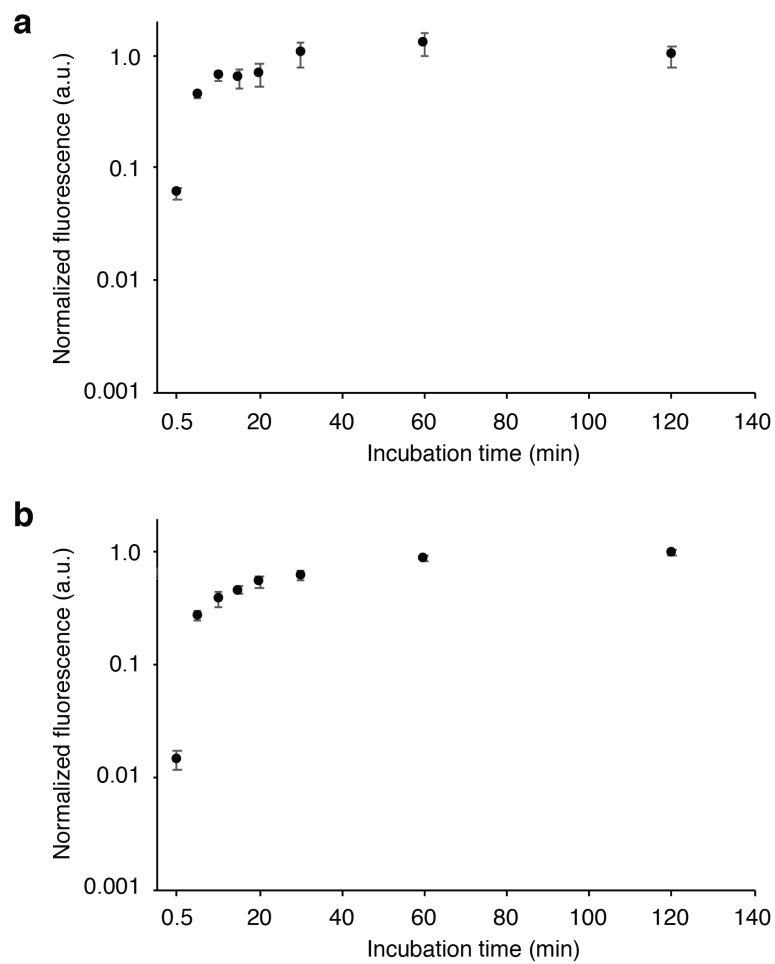
Supplementary Fig. 10

Supplementary Fig. 10 | DNA containment inside the hydrogel beads. Linear DNA fragments (977 bp) were PCR-amplified and encapsulated in the hydrogel beads at 3e9 copy/µL. Soluble DNA in the surrounding media after 72-hr incubation was quantified using qPCR. Standards were prepared by serial dilutions. Samples prepared in triplicate, data represent the mean ±1 SD. **$P = 0.0018$ (df = 4, 95% CI = -7.398 to -3.351), NS = not significant ($P = 0.1460$, df = 4, 95% CI =-2.035 to 0.4334). Statistics are derived using a two-tailed t-test. Lower limit of detection (LLOD) = 3 copy/µL.

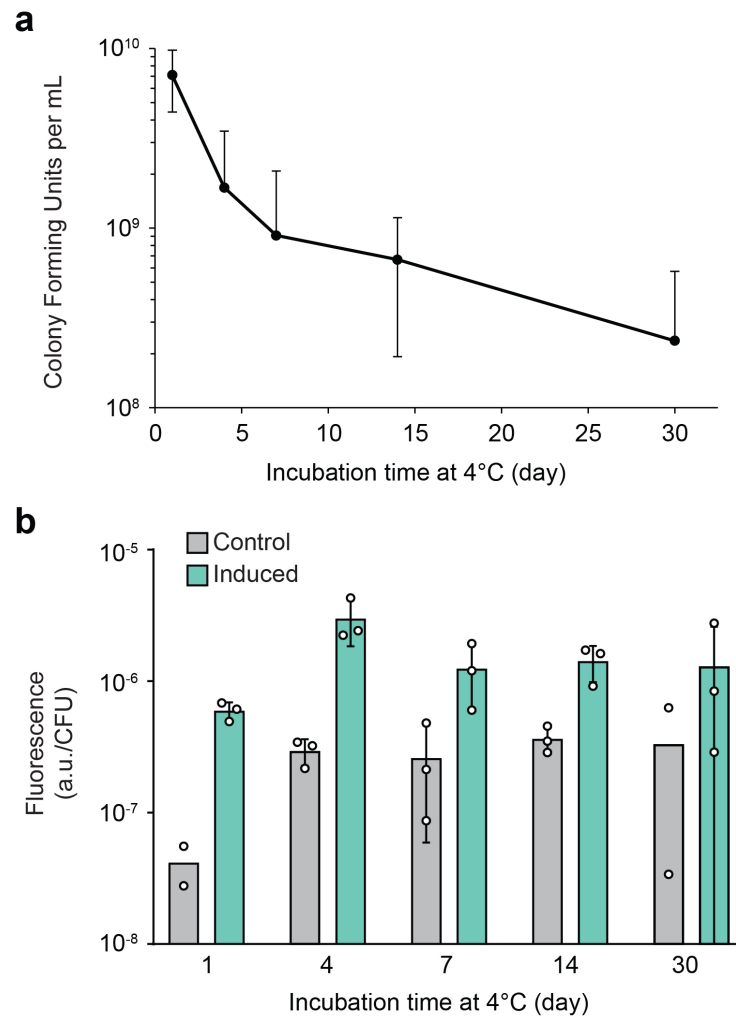Supplementary Fig. 11

a

b

Supplementary Fig. 11 | Viability of encapsulated cells at pH 4. (a) Survival rates of cells encapsulated in alginate cores of different sizes after 4 hours of shaking incubation at pH 4. The final diameters of the beads after outgrowth are approximately 6 mm, 6.5 mm, and 8 mm for initial core volumes of 50 μL, 100 μL, and 200 μL, respectively. Data are calculated from triplicate incubated in original LB and LB adjusted to pH 4. Samples prepared in triplicate, data represent the mean ±1 SD. **(b)** Spatial distribution of live (green) and dead (red) cells in the 50 μL alginate cores after 4 hours of shaking incubation at pH 4. Depth of Z-stack is 580 μm for the control bead images and 800 μm for the pH 4 bead images. Images are representative of duplicates of similar results.

a

b

Supplementary Fig. 12 | Diffusion of small molecules into the hydrogel beads. (a) Diffusion of a positively charged dye, rhodamine, into the hydrogel beads over a course of two hours. **(b)** The diffusion profile of a negatively charged dye, fluorescein. Samples prepared in triplicate, data represent the mean ±1 SD.

a

b

Supplementary Fig. 13 | Cell survival and inducibility after storage at low temperature. (a) CFU counts for cells retrieved from hydrogel beads after storage in a refrigerator (4°C) across 30 days **(B)** Comparison of aTc-induced fluorescence profiles of retrieved cells after storage at 4°C for various time periods. Samples prepared in triplicate (duplicate for the control group on day 1 and 30), data represent the mean ±1 SD.
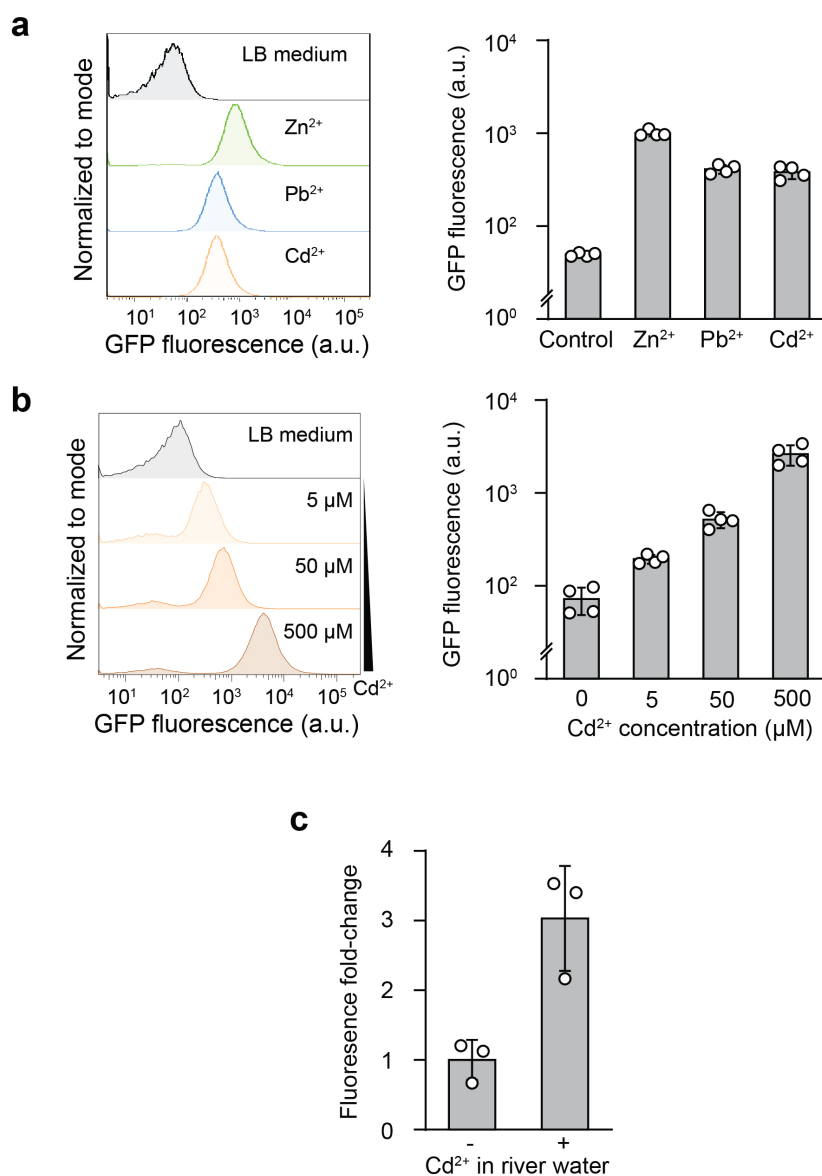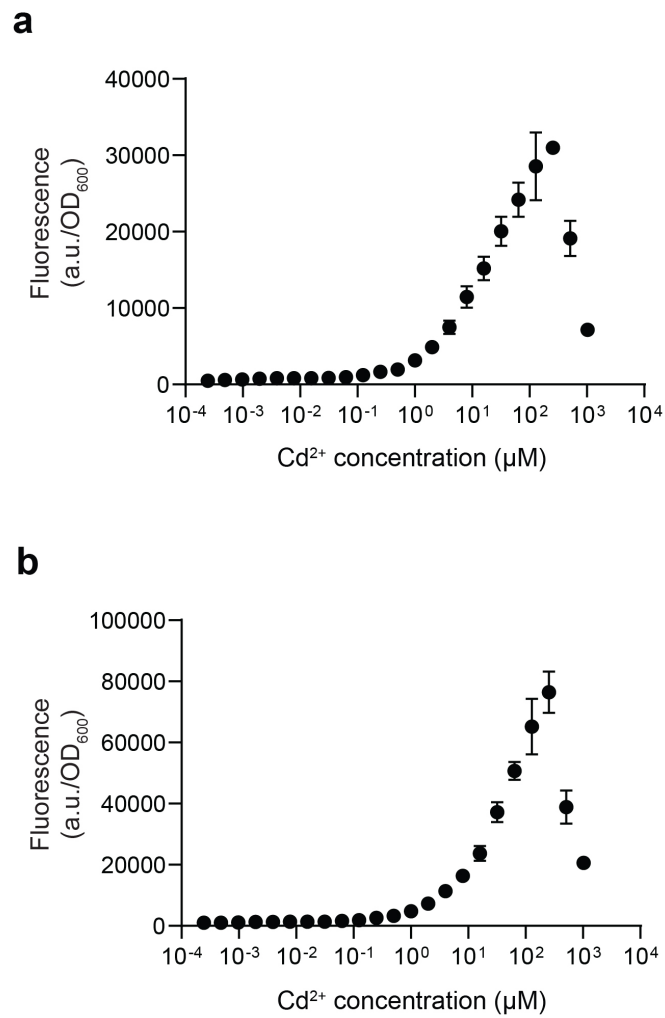
Supplementary Fig. 14
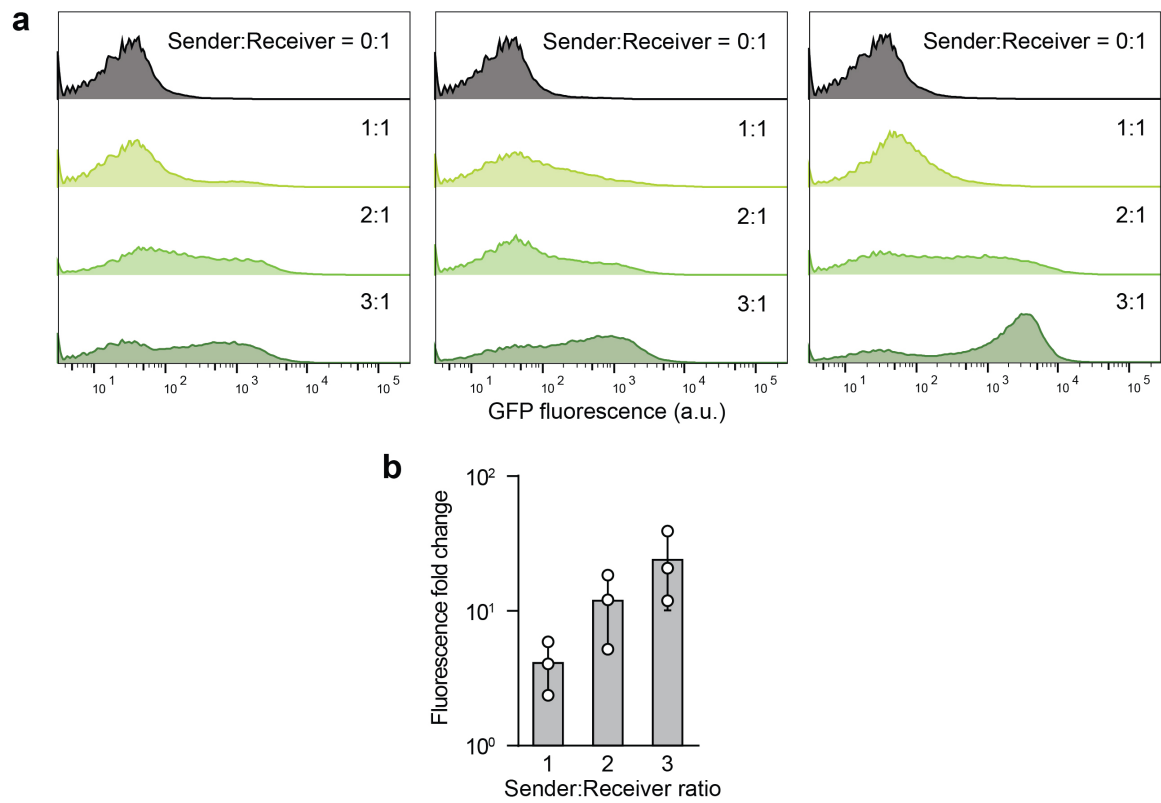
Supplementary Fig. 14 | Induction of AHL receiver beads by AHL sender beads. (a) Flow cytometry data of cells retrieved from receiver beads showed various levels of induction corresponding to different AHL sender bead to AHL receiver bead ratios (normalized to unit distribution, three biological replicates). **(b)** Fluorescence fold change of the receiver beads. Samples prepared in triplicate, data represent the mean ±1 SD.

Supplementary Fig. 15 | Heavy metal sensing in Charles River water samples. (a) Left: Flow cytometry analysis of the heavy-metal-sensing strain. Bacteria in liquid were exposed for 3 hours to 300 μM ZnCl$_2$, 100 μM Pb(NO$_3$)$_2$, and 10 μM CdCl$_2$ in LB media, respectively. Right: Mean GFP fluorescence of the heavy-metal-sensing strain. Samples prepared in n = 4 beads for each condition, data represent the mean ±1 SD. **(b)** Left: Response of the heavy-metal-sensing strain encapsulated in the tough hydrogel capsule to 0 μM, 5 μM, 50 μM, and 500 μM CdCl$_2$ after 3 hours of incubation. Right: Mean GFP fluorescence of the heavy-metal-sensing strain encapsulated in the tough hydrogel capsule. Samples prepared in n = 4 beads, data represent the mean ±1 SD. **(c)** GFP fluorescence fold-change of encapsulated cells responding to cadmium ions in Charles River water. Samples prepared in n = 3 beads, data represent the mean ±1 SD.

a

b

Supplementary Fig. 16 | Dose-response curves of P*zntA*-GFP induced by Cd^{2+}. The expression of GFP in cells harboring the plasmid pEZ074 after **(a)** 3 hours and **(b)** 6 hours of incubation with Cd^{2+}. Slow cell growth and reduced fluorescence were observed at [Cd^{2+}] > 256 μM. Samples prepared in triplicate, data represent the mean ±1 SD.

Supplementary Fig. 17

Supplementary Fig. 17 | Plasmid maps of pEZ055, pEZ058, and pEZ074. ColE1 rep: ColE1 origin of replication; amp marker: resistance gene cassette for carbenicillin; gfp: green fluorescence protein.

Supplementary Fig. 18
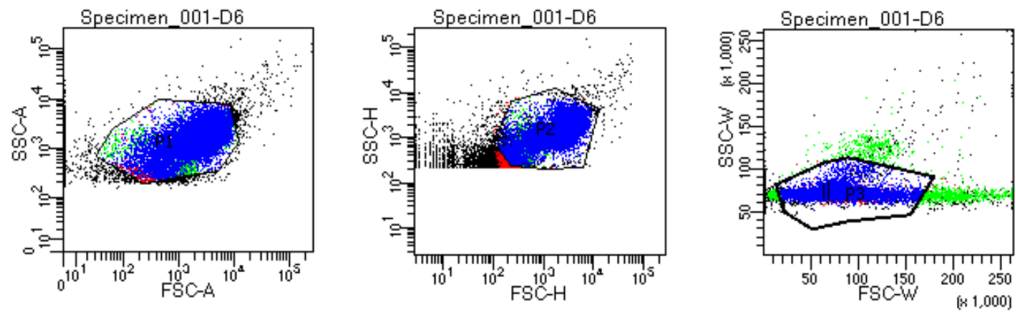
Population	#Events	%Parent	FITC-A Mean	FITC-A Median
■ All Events	33,967	####	1,103	634
■ P1	30,000	88.3	1,214	823
■ P2	29,693	99.0	1,227	841
■ P3	28,383	95.6	1,252	876

Supplementary Fig. 18 | Gating strategy for flow cytometry. Top: Cells were gated using log forward scatter area (FSC-A) by log side scatter area (SSC-A), followed by gating on log forward scatter height (FSC-H) by log side scatter height (SSC-H), and subsequent gating on log forward scatter width (FSC-W) by log side scatter width (SSC-W). Bottom: Cell population abundance during each gating stage, in numbers and percentages.

References

1. Rovner, A. *et al.* Recoded organisms engineered to depend on synthetic amino acids. *Nature* **518**, 89–93 (2015).

2. Farzadfard, F. & Lu, T. K. Genomically encoded analog memory with precise in vivo DNA writing in living cell populations. *Science (80-.).* **346**, 1256272–1256272 (2014).

3. Chen, A. Y. *et al.* Synthesis and patterning of tunable multiscale materials with engineered cells. *Nat. Mater.* **13**, 515–523 (2014).

4. Mimee, M. *et al.* An ingestible bacterial-electronic system to monitor gastrointestinal health. *Science (80-.).* **360**, 915–918 (2018).

5. Farzadfard, F. *et al.* Single-nucleotide-resolution computing and memory in living cells. *Mol. Cell* **75**, 769–780 (2019).

6. Tomović, N. S., Trifković, K. T., Rakin, M. P., Rakin, M. B. & Bugarski, B. M. Influence of compression speed and deformation percentage on mechanical properties of calcium alginate particles. *Chem. Ind. Chem. Eng. Q.* **21**, 411–417 (2015).

7. Liu, X. *et al.* Ingestible hydrogel device. *Nat. Commun.* **10**, 1–10 (2019).